https://doi.org/10.5194/egusphere-2026-4962
Preprint. Discussion started: 25 August 2026

Stable isotope proxies from Aotearoa New Zealand peatlands and their potential for reconstructing Southern Annular Mode variability

Thomas P. Roland[1*], Matthew J. Amesbury[2], Jessica Royles[3], Howard Griffiths[3], Rewi M. Newnham[4], Andrew B. H. Rees[4], Joshua L. Ratcliffe[5,6,7], David I. Campbell[5], Elizabeth D. Keller[8,9], W. Troy Baisden[5], Max Berkelhammer[10], Marco Aquino-Lopez[11], Dan J. Charman[1]

[1] Geography, Faculty of Environment, Science and Economy, University of Exeter, Exeter, UK
[2] Research Services, University of Exeter, Exeter, UK
[3] Department of Plant Sciences, University of Cambridge, Cambridge, UK
[4] School of Geography, Environment and Earth Sciences, Victoria University of Wellington, Wellington, Aotearoa New Zealand
[5] School of Science, University of Waikato, Hamilton, Aotearoa New Zealand
[6] Department of Forest Ecology and Management, Swedish University of Agricultural Sciences, Umeå, Sweden
[7] Unit for Field-Based Forest Research, Swedish University of Agricultural Sciences, Vindeln, Sweden
[8] National Isotope Centre, Earth Sciences New Zealand, Lower Hutt, Aotearoa New Zealand
[9] Antarctic Research Centre, Victoria University of Wellington, Aotearoa New Zealand
[10] Earth and Environmental Sciences, The University of Illinois Chicago, Chicago, USA
[11] CIMAT, the Mathematics Research Center in Guanajuato, Mexico

Correspondence to: Thomas Roland (t.p.roland@exeter.ac.uk)

Abstract. Peatlands dominated by the wire rush *Empodisma* spp. are widely distributed across Aotearoa New Zealand and hold considerable potential as archives for reconstructing past variability in the Southern Annular Mode, the dominant mode of Southern Hemisphere climate variability. However, the mechanistic links between climate, hydrology, and stable isotope signals in *Empodisma* cellulose remain incompletely understood. Here, using spatial (13 sites) and temporal (monthly, two sites) datasets, we examine the environmental controls on *Empodisma* cellulose $\delta^{13}C$ and $\delta^{18}O$ and their suitability for palaeoclimate reconstruction. We confirm strong spatial relationships between $\delta^{13}C$ and temperature across the Aotearoa New Zealand latitudinal transect, consistent with carbon isotope discrimination theory under non-water-limited conditions and demonstrate that moisture variables exert no significant site-scale control, although a secondary within-site relationship with water-table depth is resolved. For $\delta^{18}O$, we show that internal root and shoot waters are systematically offset from root-associated water, with a species-dependent offset (*Empodisma robustum* > *E. minus*), and that the mean of internal root and shoot water is the best-performing source for predicting root cellulose $\delta^{18}O$ in a mechanistic model. Isotope mixing modelling reveals that root water is the dominant contributor to cellulose oxygen, but that this partitioning varies systematically with season and species. Initial downcore analysis at North and South Island sites records coherent multi-decadal trends in both proxies whose relative amplitudes follow the species-dependent partitioning predicted by the modern calibration. Once corrected for the atmospheric Suess effect, however, both proxies enrich over the industrial period in the direction that would be expected from rising CO_2 rather than from circulation change, indicating that pre-industrial records

https://doi.org/10.5194/egusphere-2026-4962
Preprint. Discussion started: 25 August 2026

will be required to isolate a SAM signal. These results provide a mechanistic basis for interpreting *Empodisma* cellulose isotope records as proxies for past temperature and atmospheric circulation variability across the Southern Hemisphere mid-latitudes.

1. Introduction

1.1. Palaeoclimatic context for proxy development

The Southern Annular Mode (SAM) is the dominant mode of climate variability in the Southern Hemisphere, expressed as sea-level pressure anomalies of opposite sign between the mid-latitudes (~40° S) and high latitudes (~65° S). Shifts in the SAM drive changes in the strength and position of the Southern Hemisphere westerly winds (SHWW), which exert a major influence on temperature and precipitation patterns across mid- to high-latitude regions (Fletcher and Moreno, 2012; Fogt and Marshall, 2020; Gillett et al., 2006). The SAM is also a key component of the global climate system, affecting atmosphere-ocean CO_2 exchange (Hodgson and Sime, 2010), and the strength and variability of the Southern Ocean carbon sink (Gruber et al., 2018; Landschützer et al., 2015; McKinley et al., 2016; Saunders et al., 2018; Stewart et al., 2020), resulting in modulation of Southern Hemisphere atmospheric CO_2 concentrations (Fletcher et al., 2018; Fletcher and Moreno, 2011; Moreno et al., 2010).

Since the 1950s the SAM has trended towards its positive phase, marked by a strengthening and poleward shift of the SHWW (Gillett et al., 2006). This trend has been attributed primarily to stratospheric ozone depletion, amplified by greenhouse gas forcing (Arblaster and Meehl, 2006; Banerjee et al., 2020). However, climate models vary in their ability to reproduce the observed variability and to simulate the SAM's response to external forcing (Fogt and Marshall, 2020; Ivanciu et al., 2021). This remains a significant uncertainty in projections of Southern Hemisphere climate change.

Developing robust reconstructions of Holocene SAM variability at multi-decadal to millennial timescales is therefore essential both to constrain the dynamics of the SHWW and to provide a benchmark for testing climate model performance (Hessl et al., 2017). Yet reconstructions remain scarce: tree-ring (Lara et al., 2008; Villalba et al., 2012) and ice-core records (Abram et al., 2014; Koffman et al., 2014), alongside multi-proxy compilations (Dätwyler et al., 2018; Zhang et al., 2015), extend back up to two millennia, with recent syntheses further emphasising the potential of Common Era reconstructions (King et al., 2023). In addition, centennial- to millennial-scale reconstructions from lakes and peatlands are concentrated almost exclusively in southern South America and on the sub-Antarctic islands (Fletcher and Moreno, 2011, 2012; Frugone-Álvarez et al., 2017; Moreno et al., 2010, 2014, 2018; Perren et al., 2020; Strother et al., 2015; Xia et al., 2018). Despite these advances, Holocene SAM evolution remains poorly constrained and regionally inconsistent, with sometimes contradictory results (Hessl et al., 2017; Moreno et al., 2014), underscoring the urgent need for new proxies from SAM-sensitive regions across all sectors of the Southern Ocean.

Here we address that gap by developing a contemporary isotopic calibration for *Empodisma*-dominated restiad peatlands across a latitudinal transect of Aotearoa New Zealand, and testing its application to downcore records.

https://doi.org/10.5194/egusphere-2026-4962
Preprint. Discussion started: 25 August 2026

1.2. Regional setting

Please note that we use the term Aotearoa New Zealand to acknowledge te reo Māori and the mana whenua of the lands and waters in which this research is situated. We use the full term throughout the text. Where space is constrained, in figures and tables, we may abbreviate to 'NZ', following a common government style convention to abbreviate after the first full mention (Mathison, 2021); this is not intended to diminish the significance of Aotearoa as a place. Ngā mihi nui ki ngā tāngata whenua o Aotearoa, me ngā whenua me ngā wai i mahia ai tēnei rangahau. We acknowledge with respect the tangata whenua of Aotearoa, and the lands and waters where this research was carried out; this work would not have been possible without their support.

Aotearoa New Zealand lies in the zone of interaction between the Southern Hemisphere westerly winds (SHWW) and subtropical moisture sources (Ummenhofer and England, 2007), making it highly sensitive to changes in the SAM. These competing influences create strong latitudinal and orographic gradients in the isotopic composition of precipitation, driven by shifts in air-mass source, altitude, and rainout effects (Fig. 1). Modern climate observations show robust correlations between the SAM and Aotearoa New Zealand temperature and precipitation (Kidson, 2000; Kidston et al., 2009; Thompson et al., 2011; Ummenhofer et al., 2009). The positive phase of the SAM is associated with anomalously warm conditions throughout much of the country (Kidston et al., 2009) and with an orographic east-west precipitation contrast across the South Island, with reduced precipitation in the western side of the Southern Alps and increased precipitation in the east under positive SAM phases, and the reverse pattern under negative phases (Ummenhofer et al., 2009) SAM variability accounts for a substantial fraction of late twentieth-century summer precipitation decline in Aotearoa New Zealand (Ummenhofer et al., 2009), and seasonal asymmetries in SAM forcing are expressed in long-term station records of temperature and rainfall (Kidson, 2000). In Aotearoa New Zealand, however, the isotopic expression of these circulation changes depends not simply on rainfall amount, but on the relative contribution of subtropical versus higher-latitude moisture sources (see Sect. 1.3). These large-scale relationships are reinforced by evidence of SAM's influence on river flow variability (Li and McGregor, 2017), its role in driving extreme heat and precipitation anomalies during recent summers (Salinger et al., 2019) and high-resolution simulations that capture SAM's imprint on Aotearoa New Zealand weather extremes (Gibson et al., 2023).

Palaeoclimate records from Aotearoa New Zealand that provide insight into Holocene SAM and SHWW dynamics include radiocarbon-dated subfossil trees (Turney et al., 2016), fjord sediments (Hinojosa et al., 2017), and lake sediment records (Anderson et al., 2018; Jara et al., 2015; Turney et al., 2017). Recent syntheses emphasise the importance of the region for testing Southern Hemisphere climate teleconnections (Dätwyler et al., 2018; Gallant et al., 2013), and the potential of stable isotope analysis to address such questions has been demonstrated in speleothems (Lorrey et al., 2020), and framed by recent reviews on water-isotope process linkages across archives (Dee et al., 2023).

Holocene-spanning peatlands are widely distributed across Aotearoa New Zealand and have been shown to hold considerable potential for palaeoclimate reconstruction (Jara et al., 2017; Newnham et al., 2019). Recent work highlights their sensitivity to climate forcing, including new peat formation during warming and deglaciation in the Southern Alps

https://doi.org/10.5194/egusphere-2026-4962
Preprint. Discussion started: 25 August 2026

(Fewster et al., 2025). Yet, despite this evidence, they remain comparatively underexplored as archives for investigating past SAM variability. Moreover, although initial studies demonstrated promise, their potential as stable isotope archives for reconstructing palaeohydrological and climatic change remains largely untapped (Amesbury et al., 2015a, b).

1.3. Isotope proxies in peatland systems

Developing robust insights into past SAM behaviour requires proxies for both temperature and precipitation to resolve regional variations in climate responses and drivers, including the dynamic interaction between SAM and the El Niño-Southern Oscillation (ENSO) (Clem and Fogt, 2013; Lim et al., 2016; Vera and Osman, 2018). Recent work shows that SAM-ENSO teleconnections are often non-stationary and vary across centennial-millennial timescales, complicating reconstructions and underscoring the need for multi-proxy, process-informed approaches (Dätwyler et al., 2018, 2020; Rahaman et al., 2019).

Stable isotopes of carbon and oxygen are widely used palaeoclimate proxies in peatland research (Bilali et al., 2013; Daley et al., 2010; Jones et al., 2019; Loisel et al., 2010; Roland et al., 2015). Much of this work has been undertaken in *Sphagnum*-dominated peatlands, common in northern Europe, North America, and southern South America, where modern process studies show that cellulose $\delta^{13}C$ and $\delta^{18}O$ respond to hydrological gradients such as water-table depth, microtopography, and seasonal moisture balance, supporting their use as palaeohydrological proxies (Daley et al., 2010; Loader et al., 2016; Loisel et al., 2010). These studies also emphasise the sensitivity of *Sphagnum* isotopes to species identity and local environmental conditions, reinforcing their value as palaeoclimate proxies but also the need for careful interpretation (Granath et al., 2018).

In Aotearoa New Zealand, by contrast, peatlands are typically dominated not by *Sphagnum* but by the wire rushes (te reo Māori: wiwi) *Empodisma robustum* and *E. minus* (Amesbury et al., 2015a, b). These species form thick peat deposits through dense root mat growth and litter inputs. Their root system is dimorphic, combining anchor roots extending to over a metre depth with a shallow, vertically oriented cluster-root mat adapted to intercepting atmospheric nutrient inputs (Clarkson et al., 2009). Strong stomatal control and high sensitivity to vapour pressure deficit confer high water-use efficiency and correspondingly low rates of evapotranspiration (Speranskaya et al., 2024; Thompson et al., 1999), and resilience to seasonal drought, in marked contrast to the water-retentive strategies of *Sphagnum* mosses. These contrasting ecohydrological traits between vascular-plant and *Sphagnum*-dominated peatlands (Speranskaya et al., 2024) have direct implications for isotope behaviour, underscoring the need for locally grounded, taxon-specific calibration to unlock their value as palaeoclimate proxies. Fewer studies have assessed palaeoclimate proxies in peatlands dominated by vascular plants (Kock et al., 2019a, b), but emerging evidence shows that species-specific isotopic behaviour in vascular plants is shaped by interspecies physiological differences (Jones et al., 2019) and decomposition dynamics (Zeh et al., 2020).

Given these complexities, proxy development must be grounded in empirical and mechanistic understanding of the modern processes that underpin palaeo-interpretation. Recent mechanistic and applied studies linking carbon assimilation and moisture status to isotopic composition are improving proxy calibration and interpretive power (Loader et al., 2016; Stelling and Yu, 2019; Túri et al., 2021).

https://doi.org/10.5194/egusphere-2026-4962
Preprint. Discussion started: 25 August 2026

We previously tested relationships between carbon ($\delta^{13}C$) and oxygen ($\delta^{18}O$) in *Empodisma* cellulose and climate-hydrological variables in Aotearoa New Zealand spatial and temporal datasets (Amesbury et al., 2015a, b). For carbon (Amesbury et al., 2015b), we found significant negative correlations between cellulose $\delta^{13}C$ and temperature, cumulative photosynthetically active radiation over the growing season (above 0°C, PAR_0), and growing degree days above 0°C (GDD_0; growing season warmth expressed as accumulated temperature over the growing season). There were no significant relationships with precipitation amount, relative humidity, soil moisture or water-table depth, suggesting a lack of growing-season water limitation and a decoupling from hydrological controls often reported for *Sphagnum*-dominated peatland systems (Loisel et al., 2009, 2010). The strength and consistency of these relationships indicated that *Empodisma* cellulose $\delta^{13}C$ may provide a useful temperature proxy. That calibration is, however, a spatial one, established across a contemporary latitudinal gradient along which atmospheric CO_2 is effectively constant. Applied downcore across the industrial period it must contend with an additional control: rising atmospheric CO2 alters carbon isotope discrimination through its effect on stomatal conductance and intrinsic water-use efficiency, independently of climate, while the accompanying decline in the $\delta^{13}C$ of atmospheric CO2 (the Suess effect) is imprinted directly on plant tissue. Neither term is present in the spatial calibration, and both must be accounted for before a downcore $\delta^{13}C$ record can be read as a temperature signal. For oxygen (Amesbury et al., 2015a), we identified strong links between the isotopic composition ($\delta^{18}O$, δD) of peat-surface waters and precipitation (empirically and via back-trajectory analysis). The transfer to cellulose $\delta^{18}O$ was less clear and likely limited by a paucity of true internal-water measurements, although mechanistic modelling predicted mean cellulose values within published error margins for both spatial and temporal datasets. These findings motivated further process-based calibration of vascular-plant peat proxies and support expanding beyond *Sphagnum*-dominated systems.

1.4. Research aims

Here, we build on that earlier work by implementing a more detailed mechanistic experimental approach to refine carbon and oxygen isotope proxies in *Empodisma*. In doing so, we provide a stronger foundation for applying these proxies to late-Holocene Aotearoa New Zealand *Empodisma*-dominated peatland cores, extend peatland palaeoclimate reconstruction beyond *Sphagnum*-dominated systems, and support improved interpretation of past SAM variability. Specifically, we test the following four hypotheses:

H1: Previously observed relationships between *Empodisma* carbon and oxygen stable isotopes and the environment (Amesbury et al., 2015a, b) are replicated within a framework of expanded spatial and temporal sampling, strengthening original conclusions.

H2: Root-associated water (squeezed from the interstitial water of surface *Empodisma* root samples) and true internal plant waters (obtained via vacuum distillation) are linearly related, and this relationship provides better understanding of the isotope fractionation processes in *Empodisma*, specifically the link between source water and root cellulose.

H3: True internal root, shoot or a combination of root and shoot water is a better predictor of root cellulose $\delta^{18}O$ values than root-associated water or precipitation in a mechanistic model.

https://doi.org/10.5194/egusphere-2026-4962
Preprint. Discussion started: 25 August 2026

H4: Downcore cellulose $\delta^{13}C$ and $\delta^{18}O$ from contrasting sites behave as predicted by the surface calibration, and can be compared meaningfully against the instrumental SAM index.

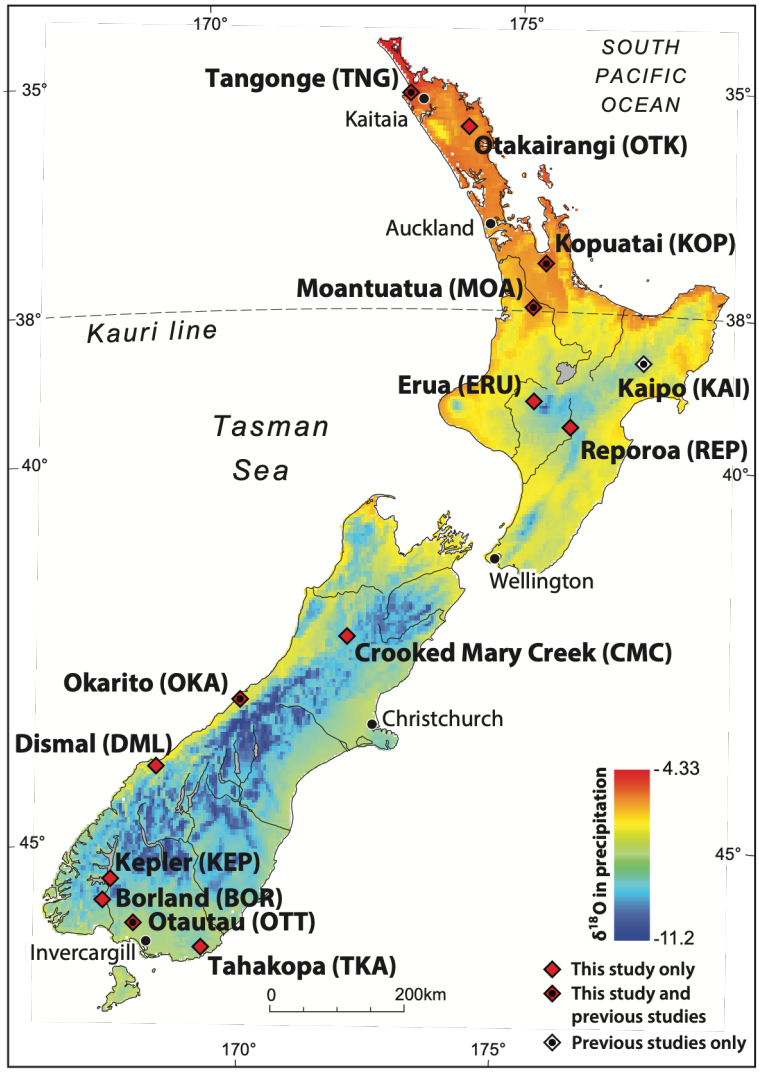

Figure 1. Locations of peatland sites included in this study and in combined analyses with previously published data. Symbols distinguish sites sampled in this study and previous studies (Amesbury et al., 2015a, b). The Kauri Line marks the geographic division between the two *Empodisma* species, with *E. robustum* north of 38° S and *E. minus* south of 38° S (Wagstaff and Clarkson, 2012). The basemap shows the annually weighted mean $\delta^{18}O$ in precipitation (‰) for 1997-2013, derived from isoscape modelling (Baisden et al., 2016).

Name	Code	Lat (°)	Long (°)	Altitude (m)	WTD range (min - max) (cm)	WTD mean (cm)	Temperature (°C)		Precipitation (mm)		Relative humidity (RH)	Isoscape mean annual $\delta^{18}O$ (‰) in ppt (SD)	Isoscape mean annual δD (‰) in ppt (SD)	GDD_0 (°C)	PAR_0 (mol photons m^{-2} $season^{-1}$)
							Mean annual	Mean summer (DJF)	Total annual	Total summer (DJF)					
Tangonge	TNG	-35.104	173.215	10	17 (30 - 47)	37.1	15.9	19.2	1319	257	84.1	-4.32 (1.16)	-23.18 (6.94)	5770	10058
Otakairangi	OTK	-35.596	174.175	95	19 (32 - 51)	43.7	15.1	18.8	1705	327	85.0	-5.09 (1.04)	-29.19 (6.48)	6081	9965
Kopuatai	KOP	-37.386	175.551	5	15 (3 - 18)	9.0	14.7	19.1	1190	242	82.7	-5.09 (1.23)	-30.35 (7.95)	5356	9739
Moanatuatua	MOA	-37.924	175.370	60	21 (61 - 82)	71.0	13.7	18.0	1191	255	84.7	-5.29 (1.23)	-30.46 (7.81)	4960	9616
Erua	ERU	-39.179	175.400	725	35 (10 - 45)	23.7	9.5	14.1	2089	437	85.1	-7.50 (1.02)	-46.62 (7.66)	3943	8699
Reporoa	REP	-39.585	176.130	1150	16 (54 - 70)	64.0	9.2	13.9	1424	313	82.1	-8.08 (1.23)	-52.31 (9.44)	4953	9185
Crooked Mary Creek	CMC	-42.399	172.133	445	22 (10 - 32)	17.2	9.4	14.6	2543	599	85.9	-7.57 (0.96)	-50.88 (8.21)	2212	7805
Okarito	OKA	-43.247	170.219	75	19 (8 - 27)	15.8	11.7	15.2	3343	879	87.6	-6.53 (1.18)	-43.62 (8.05)	4277	9282
Dismal	DML	-44.033	168.751	15	11 (7 - 18)	11.7	12.4	16.8	4215	1116	85.4	-6.39 (1.37)	-41.89 (10.21)	2148	7785
Kepler	KEP	-45.524	167.677	225	14 (22 - 36)	29.7	9.6	14.2	1102	278	82.7	-7.72 (1.27)	-51.81 (10.19)	4211	8602
Borland	BOR	-45.781	167.559	180	4 (21 - 25)	23.2	9.5	14.0	1197	297	83.4	-7.80 (1.24)	-53.41 (9.82)	4211	8602
Otautau	OTT	-46.134	168.045	65	3 (16 - 19)	17.7	10.0	14.1	1051	275	83.3	-7.34 (1.34)	-50.37 (10.23)	3627	8506
Tahakopa	TKA	-46.534	169.435	5	16 (21 - 37)	28.3	9.7	13.1	1312	322	83.0	-7.24 (1.26)	-50.07 (9.29)	4421	8769

Table 1. Study site details. Water table depth (WTD) values were measured at the time of sampling for the spatial dataset. Temperature, precipitation, and relative humidity (RH) are 1972-2013 mean values (precipitation as annual sums) from the NIWA VCSN (see Sect. 2.3). Isoscape values for $\delta^{18}O$ and δD in precipitation (ppt) are 1997-2012 annual means. Cloudiness data used to calculate PAR_0 were extracted from Kaplan et al. (2003). GDD_0 = cumulative growing degree days above 0°C. PAR_0 = cumulative photosynthetically active radiation during the growing season. SD = standard deviation. Combined analyses presented elsewhere in the manuscript also incorporate previously published data from six pilot-study sites (Amesbury et al., 2015a, b), five of which were resampled here (TNG, KOP, MOA, OKA, OTT); the remaining site (Kaipo, KAI) was not resampled and is therefore not included in this table.

https://doi.org/10.5194/egusphere-2026-4962
Preprint. Discussion started: 25 August 2026

2. Methods

2.1. Field sites and sampling

In keeping with previous work (Amesbury et al., 2015a, b), we employed both spatial and temporal sampling approaches. For both datasets, at each sampling point, two replicate sets of *Empodisma* spp. plant samples (surface-growing cluster roots and recent shoot growth, collected as paired root-shoot samples from the same plants), two water samples (one from the surface or below-ground water table, hereafter 'bog water', and one from interstitial water squeezed from cluster roots, hereafter 'root-associated water'), and a water-table depth measurement were taken. One set of plant samples was sealed in zip-lock bags for subsequent cellulose extraction, while the other set were sealed in double-capped glass vials with pierceable septa to avoid post-sampling evaporation and were retained for laboratory extraction of internal water from roots and shoots (Sect. 2.2).

For the spatial dataset, we sampled 13 *Empodisma*-dominated peatlands (five of which were also included in Amesbury et al., 2015a, b), spanning the range of precipitation isotope variability across Aotearoa New Zealand (Table 1, Fig. 1). Four sites north of the 'Kauri Line' (38° S; Tangonge, Otakairangi, Kopuatai and Moanatuatua) contained *E. robustum*, whereas all southern sites contained *E. minus* (Wagstaff and Clarkson, 2012). To ensure precipitation was the dominant moisture source, we targeted ombrotrophic peatlands (Amesbury et al., 2015a), defined either by prior knowledge (Campbell et al., 2014; Charman, 1997; Elliot, 1998; Newnham et al., 1995) or in-field using vegetation, pH and topographic indicators. Nonetheless, as in previous work (Amesbury et al., 2015a), we acknowledge that local groundwater inputs (e.g. at Erua and Crooked Mary Creek) cannot be entirely excluded. Spatial sampling was carried out in March 2016 and March 2017. Three replicate samples were analysed at each site, yielding a total dataset of 39 samples.

For the temporal dataset, monthly samples were taken from March 2016 to March 2017 at two sites representing relatively enriched (Moanatuatua, North Island) and depleted (Otautau, South Island) isotopic signatures (Fig. 1). At Moanatuatua, water-table depth was calculated daily from half-hourly readings recorded by a pressure transducer (WL1000 W, Hydrological Services, NSW, Australia) installed in a perforated PVC dip-well within 100 m of the sampling points. At Otautau, where no equivalent monitoring was available, water-table depth was measured monthly at two locations adjacent to the sampling sites. Precipitation was collected monthly at both sites using a standard method (Daley et al., 2010): a stainless-steel funnel directed rainfall into a large container with a thin film of paraffin oil to prevent evaporative enrichment. Containers were rinsed and the paraffin oil film renewed after each collection.

2.2. Water and cellulose isotopic analyses

Internal root and shoot waters were extracted from the sealed plant samples (Sect. 2.1) using cryogenic vacuum distillation (Ehleringer et al., 2000; West et al., 2006). Externally adhering water was removed from root material prior to extraction, so that extracted water represents the internal tissue pool. Samples were frozen in liquid nitrogen, then heated with hot water. The resulting tissue water sublimated through a needle into an evacuated distillation line and condensed into a vial externally

https://doi.org/10.5194/egusphere-2026-4962
Preprint. Discussion started: 25 August 2026

cooled by liquid nitrogen. Distillation was continued until the vacuum returned to its initial value. The system was then opened to atmospheric pressure, the frozen water sample melted, and the water transferred to a 2 mL vial.

Isotopic analyses of all water samples ($\delta^{18}O$ and δD) were carried out at the Lancaster Environment Centre, UK. Prior to analysis, samples were filtered through glass wool to remove particulates introduced during sampling. $\delta^{18}O$ was measured by pyrolysis of 0.5 µL of water at 1450°C over glassy carbon, and δD was determined by reducing 1 µL of water to hydrogen gas at 1080°C over a chrome-based catalyst, using a Vario Pyrocube (Elementar Analysensysteme, Germany) interfaced with an Isoprime100 isotope ratio mass spectrometer (Isoprime, UK). Internal (LEC tap water) and international standards (VSMOW2, IAEA; Low Water, Elemental Microanalysis, UK) were run with each batch. Analytical precision was 0.5 ‰ for $\delta^{18}O$ and 1 ‰ for δD.

Cellulose was extracted from cleaned roots and shoots (Amesbury et al., 2015a, b) following a standard bleaching procedure (Daley et al., 2010; Loader et al., 1997). Isotopic analyses of cellulose were performed at the Godwin Laboratory (Department of Earth Sciences, University of Cambridge). For $\delta^{18}O$, 0.1 mg subsamples of dried cellulose, sealed in silver capsules (5.25 × 3.2 mm), were analysed by pyrolysis using a Thermo Finnigan TC/EA coupled to a Thermo Delta V mass spectrometer via a ConFlo III interface. Two laboratory standards (α-cellulose and CC31) and an international standard (NBS 127) were used to calibrate the reference gas and anchor $\delta^{18}O$ to the VSMOW scale. Analytical precision was better than 0.4 ‰.

For $\delta^{13}C$, 1 mg cellulose subsamples were sealed in tin capsules (5.25 × 3.2 mm) and combusted using a Costech Elemental Analyser interfaced with a Thermo MAT 253 mass spectrometer in continuous-flow mode. Ratios were measured relative to the VPDB standard, with analytical precision better than 0.1 ‰.

All isotope ratios are reported as per mil (‰) deviations from international standards (VSMOW for oxygen and hydrogen; VPDB for carbon), where $\delta = [(R_{sample} / R_{standard}) - 1] \times 1000$ (Coplen, 2011), and R represents $^{18}O/^{16}O$, $^{2}H/^{1}H$, or $^{13}C/^{12}C$.

2.3. Climate and isoscape data

Climate data for mean monthly temperature, relative humidity, soil moisture index, and total monthly precipitation were obtained from the Aotearoa New Zealand National Institute for Water and Atmospheric Research (NIWA) National Climate Database (cliflo.niwa.co.nz). For each site, we used the 0.05° × 0.05° gridded Virtual Climate Station Network (VCSN; Tait et al., 2012, 2006) cell to calculate long-term annual or growing season means (or sums for precipitation) for the period 1972-2013. From VCSN data we also calculated growing degree days above 0°C (GDD_0; cumulative growing-season warmth). Cumulative photosynthetically active radiation (PAR_0) was calculated using the 0.5° × 0.5° CLIMATE2.2 dataset (Kaplan et al., 2003), since cloudiness data, required for PAR_0 estimation (Prentice et al., 1992), are not available in VCSN.

To characterise spatial variation in the isotopic composition of precipitation, we used modelled isoscape values of $\delta^{18}O$ and δD from the VCSN grid square containing each site (Amesbury et al., 2015a; Baisden et al., 2016). These variables are not independent: mean annual temperature (MAT), mean summer temperature (MST), GDD_0 and PAR_0 all covary strongly

https://doi.org/10.5194/egusphere-2026-4962
Preprint. Discussion started: 25 August 2026

along the latitudinal transect. Correlations are therefore reported individually as indicators of a shared thermal-energy gradient rather than as separable controls.

2.4. IsoGSM modelling of SAM-related precipitation isotope anomalies

We used the isotope-enabled atmospheric general circulation model IsoGSM to characterise precipitation $\delta^{18}O$ anomalies associated with positive and negative phases of the SAM across Aotearoa New Zealand. IsoGSM incorporates stable water isotope tracers ($\delta^{18}O$, δD) within a nudged AGCM framework, in which large-scale atmospheric circulation is constrained by reanalysis fields, improving the representation of synoptic variability in simulated precipitation isotopes (Yang et al., 2016). Previous applications have demonstrated that IsoGSM captures key circulation controls on precipitation isotopes when evaluated against GNIP observations and regional climatologies, including synoptic-scale isotope variability in western North America (Berkelhammer et al., 2012), supporting its use as a diagnostic tool for palaeoclimate interpretation.

For this study, monthly precipitation $\delta^{18}O$ fields were extracted over Aotearoa New Zealand for the period 1979-2018. Anomalies were calculated relative to the 1979-2018 climatological mean. For both austral summer (DJF) and annual conditions, composite anomaly maps were constructed by averaging $\delta^{18}O$ values across the five years with the most positive SAM indices and the five years with the most negative SAM indices, based on the standard SAM index. Site locations are shown on the anomaly maps (Fig. 2) to highlight spatial contrasts most relevant for interpreting *Empodisma* cellulose $\delta^{18}O$ signals.

This modelling approach is intended to provide a climatological and process-oriented assessment of typical SAM-related isotopic patterns, rather than to reproduce individual precipitation events.

2.5. Mechanistic and isotope mixing model

Mechanistic modelling focused on root cellulose, which is well-preserved in *Empodisma*-dominated peats and provides the principal material for downcore palaeoenvironmental reconstruction; shoot cellulose exhibits substantially larger source water offsets (≈10 ‰), making it less suitable for proxy development (Amesbury et al., 2015a).

We applied a mechanistic model to predict *Empodisma* root cellulose values ($\delta^{18}O_c$) from source water ($\delta^{18}O_s$), following established formulations that account for the combined effects of biochemical (ε_b), equilibrium (ε_e) and kinetic (ε_k) fractionation, together with the influence of relative humidity (h) (Amesbury et al., 2015a; Daley et al., 2010; Zanazzi and Mora, 2005).

$$\delta^{18}O_c = \delta^{18}O_s + \Delta \quad (1)$$

where

$$\Delta = \varepsilon_b + (\varepsilon_e + \varepsilon_k)(1 - h) \quad (2)$$

Table 2 provides definitions of all variables. Following previous work, ε_b was set to 27 ‰ (Yakir and DeNiro, 1990) and ε_k to 28.5 ‰ (Amesbury et al., 2015a; Buhay et al., 1996); see Table 2. Equilibrium fractionation (ε_e) was calculated as a function of temperature in Kelvin. For sites dominated by *E. robustum* (TNG, OTK, KOP and MOA), mean annual

https://doi.org/10.5194/egusphere-2026-4962
Preprint. Discussion started: 25 August 2026

temperature (MAT) was used, reflecting year-round growing conditions. For all *E. minus* sites, mean summer temperature (MST; Nov-Mar) was used, reflecting more seasonal growth.

The mechanistic model was used to evaluate how well measured root cellulose $\delta^{18}O$ could be predicted from alternative candidate source waters. For the spatial dataset, candidate source waters included isoscape-modelled precipitation, root-associated water, internal root water, internal shoot water, and the unweighted (1:1) mean of internal root and internal shoot water $\delta^{18}O$. The relative contribution of the two pools was not optimised at this stage; it is quantified separately by the two-endmember mixing model described below (Sect. 2.5). For the temporal dataset, measured precipitation was used in place of isoscape-modelled precipitation.

To estimate the isotopic composition of the source water implied by measured root cellulose, Eq. (1) was rearranged as:

$$\delta^{18}O_s = \delta^{18}O_c - \Delta \quad (3)$$

We then applied a two-endmember isotope mixing model (Phillips and Gregg, 2001; Shi et al., 2019) to test whether this effective source water could be described as a mixture of internal root water (δ_A) and internal shoot water (δ_B). These two endmembers were selected as the measured plant-internal water pools most directly linked to cellulose formation, whereas precipitation and root-associated water are external or upstream pools rather than immediate internal source waters.

The isotope mixing model was defined as:

$$\delta_M = f_A\,\delta_A + f_B\,\delta_B \quad (4)$$

subject to

$$f_A + f_B = 1 \quad (5)$$

where δ_M is the isotopic composition of the mixed source water ($\delta^{18}O_s$), and f_A and f_B are the fractional contributions of internal root and internal shoot water, respectively.

In the principal formulation, a single fixed mixing ratio was fitted for the full dataset and for predefined subsets of samples by identifying the value of f_A between 0 and 1 that minimised the mean absolute error (MAE) between modelled and measured root cellulose ($\delta^{18}O_c$). For a given value of f_A, mixed source water was first calculated from Eq. (4) and then entered into the mechanistic model (Eq. 1) to generate predicted root cellulose $\delta^{18}O$. Model performance was assessed using the mean offset between modelled and measured values, the standard deviation of offsets, and the proportion of samples with absolute offsets within ± 3 ‰, corresponding to the accepted uncertainty envelope around ε_b.

To test whether source-water use varied systematically (taxa, sites, seasons), the fixed-ratio mixing model was first applied to the full spatial dataset and then repeated for predefined subsets. Spatial subsets included species groups (*E. robustum* and *E. minus*) and individual sites. For the temporal dataset, which comprised repeated sampling from MOA and OTT only, the fixed-ratio model was applied to growing-season (Nov-Mar) and non-growing (Apr-Oct) subsets, both for the combined temporal dataset and for each site separately. Additional per-sample exact-fit and zero-mean formulations were explored as sensitivity analyses.

https://doi.org/10.5194/egusphere-2026-4962
Preprint. Discussion started: 25 August 2026

Variable	Description / reference	Units
$\delta^{18}Oc$	Stable oxygen isotopic composition of *Empodisma* root cellulose; modelled values compared to measured values	‰ VSMOW
$\delta^{18}Os$	Stable oxygen isotopic composition of the effective source water used in root-cellulose formation	‰ VSMOW
Δ	Net fractionation term in the mechanistic model, where $\Delta = \varepsilon_b + (\varepsilon_e + \varepsilon_k)(1 - h)$	‰
ε_b	Biochemical fractionation factor; set to 27 ‰ (Yakir and DeNiro, 1990)	‰
ε_e	Water liquid-vapour equilibrium fractionation factor, calculated as a function of temperature (Yu, 2013; Yu et al., 2011)	‰
ε_k	Water liquid-vapour kinetic fractionation factor; set to 28.5 ‰ (Amesbury et al., 2015a; Buhay et al., 1996)	‰
h	Relative humidity, expressed as a fraction (0-1). Mean 1972-2013 NIWA VCSN h from the 0.05 × 0.05° grid square containing each site (spatial dataset) (Tait et al., 2006)	dimensionless
T	Mean growing season temperature in Kelvin (1972-2013 NIWA VCSN), used to calculate ε_e (Tait et al., 2006); MAT for *E. robustum* sites and MST (Nov-Mar) for *E. minus* sites	K
δ_M	Isotopic composition of the mixed internal source water in the two-endmember model	‰ VSMOW
δ_A	Stable oxygen isotopic composition of internal root water (endmember A)	‰ VSMOW
δ_B	Stable oxygen isotopic composition of internal shoot water (endmember B)	‰ VSMOW
f_A	Fractional contribution of internal root water to the mixed source water	dimensionless (0-1)
f_B	Fractional contribution of internal shoot water to the mixed source water; $f_A + f_B = 1$	dimensionless (0-1)

Table 2. Variables and parameters used in mechanistic model (Eqs. (1)-(3)) and two-endmember isotope mixing model (Eqs. (4)-(5)) used to interpret root-cellulose $\delta^{18}O$ in *Empodisma* spp. All δ values are expressed relative to VSMOW.

2.6. Palaeo-application: core material, chronology and isotopic corrections

Peat cores were taken from Tangonge, North Island in March 2016 (35.104° S, 173.215° E) and Otautau, South Island in March 2017 (46.134° S, 168.045° E). Root cellulose was extracted for $\delta^{13}C$ and $\delta^{18}O$ analysis at contiguous 1-cm resolution, following the extraction methods and analytical procedures described in Sect. 2.2. Total core depths were 667 cm at Tangonge and 575 cm at Otautau; however, only results since 1900 CE (equivalent to 0-31 cm at Tangonge and 0-43 cm at Otautau) are presented here, to facilitate comparison with the observed Southern Annular Mode index (Marshall, 2003; downloaded from https://legacy.bas.ac.uk/met/gjma/sam.html). Data visualisation was carried out in R using *ggplot2* and

https://doi.org/10.5194/egusphere-2026-4962
Preprint. Discussion started: 25 August 2026

patchwork packages. Primary directional trends in the isotope and SAM time-series were illustrated using LOESS smoothers (span = 0.75; 95 % confidence).

Chronological control was established using a combination of radiocarbon (^{14}C) and lead-210 (^{210}Pb) dating. ^{14}C analyses were undertaken at Direct AMS (Seattle, USA) on hand-picked, cleaned above-ground plant macrofossils (Table S1). ^{210}Pb dating was performed at the University of Exeter (UK) by alpha spectrometry following the methods of Estop-Aragonés et al. (2018). Bayesian age-depth models were constructed for both sites using the rplum package in R (Aquino-López et al., 2018). Plum integrates ^{210}Pb and ^{14}C ages within a single framework, avoiding the need to first construct an independent ^{210}Pb age model (e.g. constant rate of supply (CRS), Appleby and Oldfield, 1978). Instead, it uses raw total ^{210}Pb concentrations (Bq/kg) directly, allowing independence between datasets to be preserved. The Bayesian framework also permits natural integration of multiple dating sources (^{210}Pb and ^{14}C), providing coherent and robust age-depth models (Fig. S1).

Downcore cellulose $\delta^{13}C$ values are reported both as measured and after correction for the industrial-period decline in atmospheric $\delta^{13}C$-CO_2 (the Suess effect). Corrected values were obtained by subtracting the deviation of atmospheric $\delta^{13}C$-CO_2 at each modelled sample age from its 1850 value, using the global annual CMIP6 atmospheric $\delta^{13}C$-CO_2 compilation of Graven et al. (2017), which splices ice-core and firn records with direct atmospheric measurements from 1977 onwards and is the standard adopted for CMIP6 historical simulations. Atmospheric $\delta^{13}C$-CO_2 declines from -6.61 ‰ in 1850 to -8.44 ‰ in 2015 in this compilation; values for the two youngest samples were extrapolated linearly from the final decade of the record. Corrected values are expressed relative to that pre-industrial baseline. Analysis was restricted to samples dating from 1900 CE onwards (TNG n = 30, OTT n = 42). Because the correction removes a monotonic atmospheric trend, it does not affect the timing or relative structure of variability within each record, only the magnitude and sign of the long-term trend. All contemporary calibration $\delta^{13}C$ values are from material grown under a common modern atmosphere and are reported as measured.

2.7. Statistical analyses

Meteoric water line relationships were fitted by major axis (orthogonal) regression, which is appropriate where both variables are subject to measurement error; ordinary least squares regression is used for all other bivariate relationships. Associations between cellulose isotope values and climate variables were assessed using Pearson correlation. Interspecific comparisons used Welch two-sample t-tests, which do not assume equal variances, and root-shoot comparisons used paired t-tests. Significance was assessed at $\alpha = 0.05$ throughout, and exact p values are reported.

https://doi.org/10.5194/egusphere-2026-4962
Preprint. Discussion started: 25 August 2026

3. Results

3.1. Oxygen isotopes

3.1.1. IsoGSM precipitation $\delta^{18}O$ anomalies

To place observed precipitation $\delta^{18}O$ gradients in the context of large-scale atmospheric circulation, we first examined IsoGSM-simulated precipitation isotope anomalies, which revealed clear $\delta^{18}O$ signals associated with positive and negative phases of the SAM (Fig. 2). In general, positive SAM states are characterised by more negative $\delta^{18}O$ anomalies relative to the 1979-2018 climatology, whereas negative SAM states are associated with more positive $\delta^{18}O$ anomalies (Fig. 2A-D). The magnitude and spatial expression of these anomalies vary both seasonally and regionally across Aotearoa New Zealand. These contrasting isotope anomalies are consistent with known SAM-related circulation changes over Aotearoa New Zealand. The influence of the SAM on Aotearoa New Zealand climate is strongly seasonal: during austral summer the SAM produces a largely zonal wind-speed anomaly, whereas in winter the response is more meridional and regionally complex (Kidston et al., 2009). Broadly, positive SAM phases are associated with anomalously high pressure over Aotearoa New Zealand, lighter winds, reduced precipitation, and reduced synoptic variability, whereas negative SAM phases are associated with stronger westerlies, more frequent synoptic disturbance, and enhanced precipitation, particularly over the South Island (Kidston et al., 2009; Renwick and Thompson, 2006; Ummenhofer and England, 2007)

From an isotopic perspective, Aotearoa New Zealand precipitation $\delta^{18}O$ is strongly sensitive to the country's variable exposure to alternating subtropical and sub-Antarctic moisture sources, with warmer lower-latitude sources producing relatively enriched precipitation and cooler high-latitude Southern Ocean sources producing more depleted precipitation (Baisden et al., 2016). In that context, the more negative IsoGSM $\delta^{18}O$ anomalies during positive SAM phases (Fig. 2A, C) are consistent with a greater relative influence of cooler, higher-latitude air masses, whereas the more positive anomalies during negative SAM phases (Fig. 2B, D) are consistent with enhanced lower-latitude moisture influence. More broadly, negative SAM states have been linked to more equatorward moisture sourcing in Southern Hemisphere high-latitude precipitation, likely through amplified planetary wave activity (Gao et al., 2024), providing a plausible large-scale mechanism for this isotopic contrast. These relationships suggest that moisture source characteristics, particularly source-region latitude and temperature, represent the dominant control on precipitation $\delta^{18}O$ variability at our sites, rather than local temperature alone.

The December-February (DJF) season is emphasised because SAM anomalies exert their strongest influence on Aotearoa New Zealand climate during austral summer (Kidston et al., 2009), and because DJF represents the main growing season for the seasonally constrained *E. minus* at South Island sites. For year-round growing *E. robustum* at North Island sites, annual mean composites (Figs. 2C, D) are equally relevant for isotope incorporation, though they reproduce the same broad north-south contrast with reduced anomaly magnitudes. During positive SAM states, DJF precipitation exhibits pronounced depleted anomalies over the North Island, while anomalies are weaker across much of the South Island, particularly in the far

https://doi.org/10.5194/egusphere-2026-4962
Preprint. Discussion started: 25 August 2026

south (Fig. 2A). Negative SAM states show the opposite pattern, with strong enriched anomalies over much of the South Island and more moderate changes across the North Island, except for enrichment in the far north (Fig. 2B).

Overall, these simulated patterns are broadly consistent with observed SAM-related temperature and precipitation gradients across Aotearoa New Zealand. Critically, the moisture-provenance interpretation holds even where positive SAM phases are associated with increased precipitation frequency in northern Aotearoa New Zealand – the precipitation that falls retains the isotopically-depleted signature of higher-latitude Southern Ocean air masses rather than subtropical or Tasman Sea sources (Baisden et al., 2016; Kidston et al., 2009; Renwick and Thompson, 2006; Ummenhofer and England, 2007). The IsoGSM simulations thereby provide an interpretive framework for measured cellulose $\delta^{18}O$ values in *Empodisma*, facilitating attribution of regionally contrasting site-specific isotope records to SAM-driven changes in Southern Hemisphere atmospheric circulation.

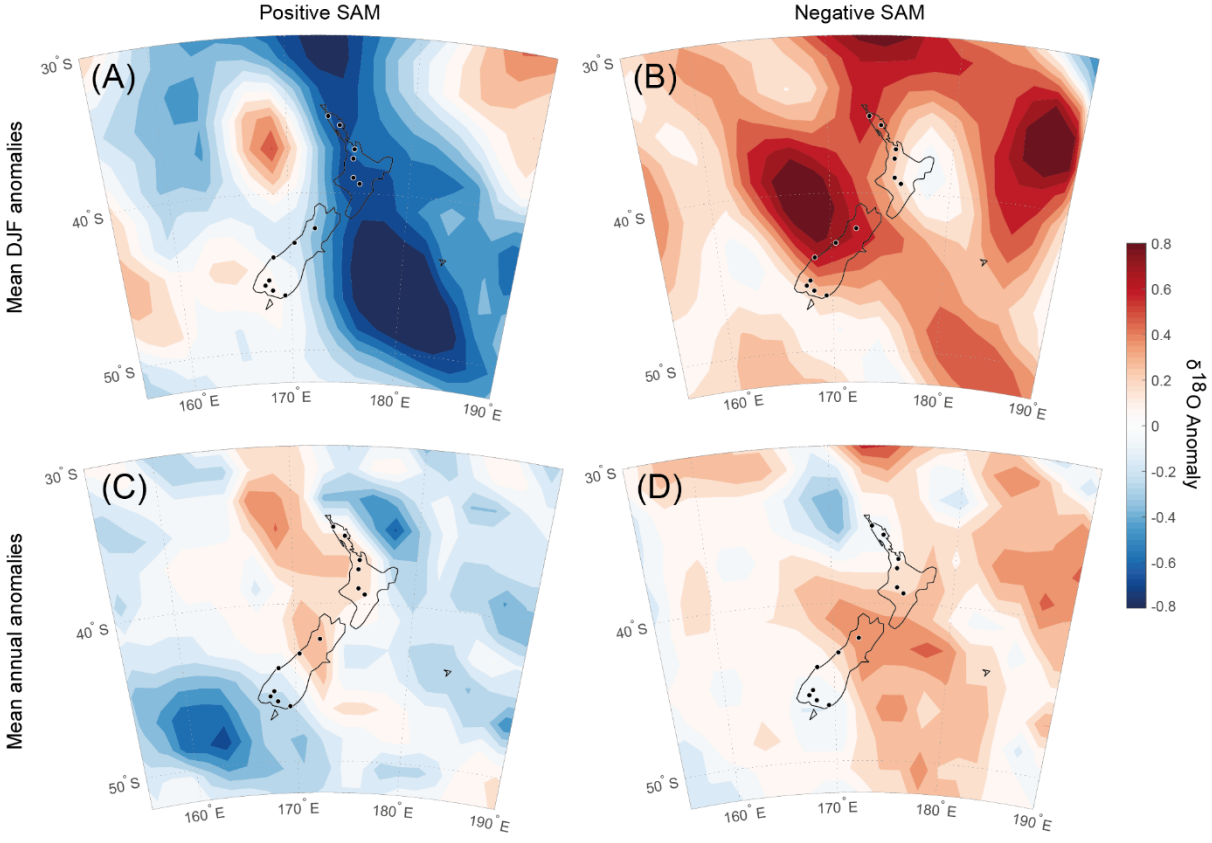

Figure 2. IsoGSM-simulated $\delta^{18}O$ anomalies in precipitation for December-February (DJF; top row, panels A-B) and annual means (bottom row, panels C-D), composited for positive SAM phases (left-hand column) and negative SAM phases (right-hand column). Each map represents the mean of the five most extreme positive or negative SAM years during 1979-2018. Black dots indicate *Empodisma* sampling sites (see Fig. 1). The anomalies are expressed relative to the 1979-2018 climatology.

https://doi.org/10.5194/egusphere-2026-4962
Preprint. Discussion started: 25 August 2026

3.1.2. Transfer of precipitation isotope signals to peatland waters

To assess how these precipitation isotope gradients are transferred into peatland hydrological systems, we compared isoscape-modelled and sampled precipitation $\delta^{18}O$ values with sampled peatland waters across the spatial and temporal datasets. Site-specific mean isoscape-modelled precipitation $\delta^{18}O$ values (Table 1) showed a significant correlation with latitude ($r = 0.708$, $p = 0.006$), indicating a pronounced north-south isotopic gradient across the study transect. More southerly sites are characterised by increasingly $\delta^{18}O$-depleted precipitation, consistent with a greater influence of cooler, higher-latitude Southern Ocean air masses and southerly to south-westerly moisture pathways, whereas northern sites receive a greater contribution from relatively $\delta^{18}O$-enriched subtropical and Tasman Sea air masses (Baisden et al., 2016; Ummenhofer and England, 2007). Superimposed on this latitudinal pattern, altitude effects are also evident, with Erua, Reporoa, and Crooked Mary Creek exhibiting more depleted $\delta^{18}O$ values than other sites at comparable latitudes (Table 1).

In $\delta^{18}O$-δD space, peatland waters plot close to the global meteoric water line (GMWL) and broadly preserve the meteoric structure of regional precipitation in both datasets (Fig. 3), with local meteoric water lines for precipitation and combined peatland waters closely paralleling the GMWL (spatial slopes: 8.51 and 8.80; temporal slopes: 8.36 and 9.10), indicating little evaporative modification at the peatland scale.

However, spatial precipitation-to-water transfer is strongest for bog water ($r = 0.724$, $p = 0.005$) and weaker for root-associated water ($r = 0.350$, $p = 0.241$), whereas temporal root-associated water tracks measured precipitation strongly overall ($r = 0.788$, $p < 0.001$) and particularly at MOA (MOA: $r = 0.910$, $p < 0.001$; OTT: $r = 0.635$, $p = 0.027$).

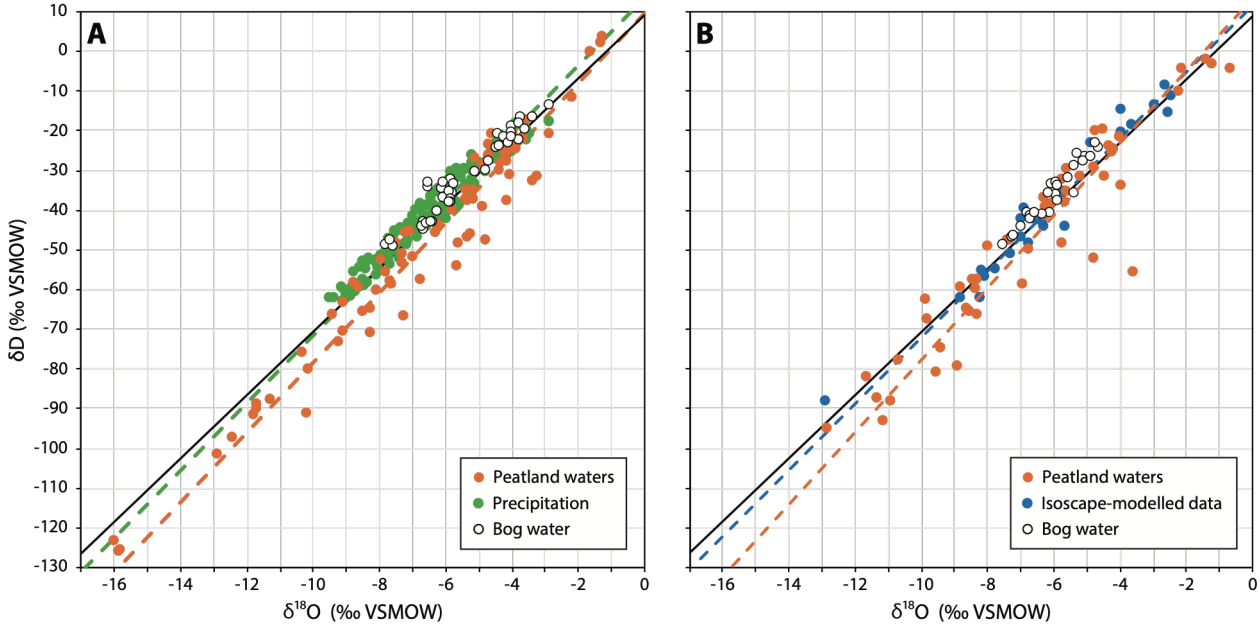

https://doi.org/10.5194/egusphere-2026-4962
Preprint. Discussion started: 25 August 2026

Figure 3. $\delta^{18}O$-δD relationships for the spatial (A) and temporal (B) datasets. In panel A, monthly isoscape-modelled precipitation values (n = 156), bog water, and combined peatland waters are shown for the 13 spatial sites. In panel B, measured precipitation from MOA and OTT, bog water, and combined peatland waters are shown for the temporal dataset. Combined peatland waters comprise root-associated water and internal root water only; internal shoot water is excluded because it is strongly modified by transpirational enrichment and plots well off the meteoric water line (Tables S2-S4). The solid black line denotes the global meteoric water line (GMWL). Dashed coloured lines show fitted local meteoric water lines for precipitation and combined peatland waters, with line colours matching the corresponding plotted datasets. Bog water is shown separately for context but is not included in the combined peatland-water fit. For consistency with the final MWL analysis, reported spatial isoscape precipitation statistics are based on site-level annual isoscape values (n = 13), whereas the monthly isoscape values are plotted in panel A to show the broader climatological distribution.

3.1.3. Root-associated water versus internal root waters

Root-associated water and internal root water show a strong positive relationship across the combined spatial and temporal datasets (Fig. 4B), indicating close coupling between external peatland water sources and internal plant water pools. However, internal root water is generally systematically isotopically depleted relative to root-associated water in both $\delta^{18}O$ and δD (Fig. 4A; Table 3). Across the combined dataset, the relationship between root-associated and internal root water was significant ($r = 0.719$, $p < 0.001$, $n = 63$; Fig. 4B). The mean offset, expressed as root-associated minus internal root water (Sect. 2.2), was 2.98 ‰ for $\delta^{18}O$ and 30.62 ‰ for δD (Table 3), indicating that internal root water is generally isotopically lighter than the associated external water pool. This pattern is consistent with systematic modification of water isotopic composition during uptake or internal transport within the plant. These data establish a consistent offset between the two pools but cannot identify the process responsible, which may reflect fractionation during uptake, differential turnover of the two pools, or incomplete equilibration between them. Spatial root-associated values for TNG5 and TNG6 were excluded from these analyses because they showed physically impossible positive $\delta^{18}O$ values and are interpreted as sampling artefacts, leaving n = 37 rather than n = 39 for spatial root-associated comparisons. The magnitude of this offset also varies between species. The mean $\delta^{18}O$ offset was greater in *Empodisma robustum* (3.89 ‰) than in *E. minus* (2.46 ‰), and a Welch two-sample t-test on absolute offset magnitude across the combined spatial and temporal datasets indicated a significant interspecific difference ($p = 0.033$; Table 3). These results show that root-associated water and internal root water are closely related but not interchangeable, and that the magnitude of the offset between them differs systematically between the two *Empodisma* species. A comparable species contrast is evident in internal shoot water, which is markedly more enriched at *E. robustum* sites (site means +3.8 to +23.5 ‰) than at *E. minus* sites (-27 to +11.8 ‰; Table S2), consistent with greater transpirational enrichment in the year-round-growing northern species.

https://doi.org/10.5194/egusphere-2026-4962
Preprint. Discussion started: 25 August 2026

	Combined (n = 63)		Spatial (n = 37)		Temporal (n = 26)	
	δD	$\delta^{18}O$	δD	$\delta^{18}O$	δD	$\delta^{18}O$
Mean	30.62	2.98	28.43	2.80	33.75	3.23
Standard deviation	15.25	2.07	13.31	1.72	17.45	2.51
Max	78.94	10.43	70.70	7.32	78.94	10.43
Min	-2.01	-2.09	2.01	-0.66	9.96	-2.09
Range	76.93	12.52	68.69	7.99	68.97	12.52
E. robustum	37.49 (19.34)	3.89 (2.41)	36.93 (16.91)	3.53 (2.11)	37.91 (21.69)	4.16 (2.66)
E. minus	26.68 (10.72)	2.46 (1.68)	25.28 (10.4)	2.54 (1.51)	29.58 (11.22)	2.31 (2.05)

485 **Table 3. Summary statistics for the isotopic offset between root-associated and internal root waters.** The offset is expressed as root-associated minus internal root water, so positive values indicate that internal root water is isotopically depleted relative to root-associated water. Values represent mean (standard deviation). Species-specific values are shown for sites dominated by Empodisma robustum and E. minus. Spatial TNG5 and TNG6 root-associated values were excluded as artefacts. Combined regression statistics are reported in the main text and Figure 4.

490

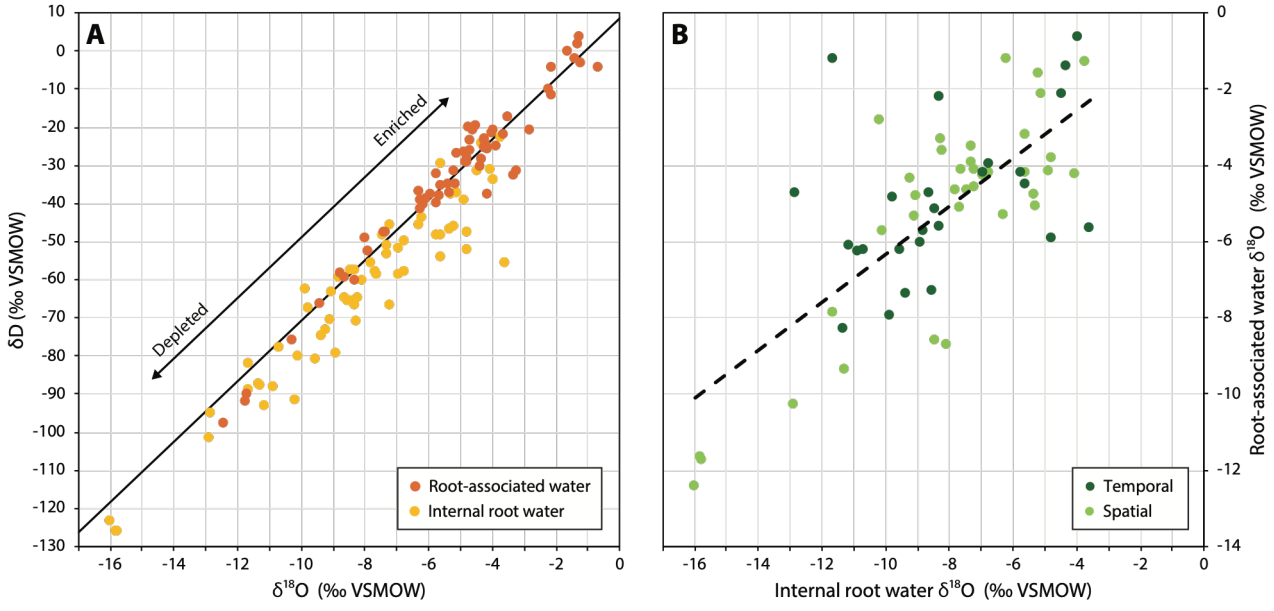

Figure 4. (A) $\delta^{18}O$-δD biplot comparing root-associated water and internal root water for the combined spatial and temporal datasets. (B) Relationship between $\delta^{18}O$ values of root-associated water and internal root water for both datasets. The solid line indicates the fitted

https://doi.org/10.5194/egusphere-2026-4962
Preprint. Discussion started: 25 August 2026

linear regression for the combined dataset ($r = 0.719$, $p < 0.001$, $n = 63$). Spatial TNG5 and TNG6 root-associated values were excluded as artefacts.

3.1.4. Mechanistic model source water comparison

Because cellulose $\delta^{18}O$ integrates both source-water isotopic composition and temperature- and humidity-dependent fractionation during evaporative enrichment and biosynthesis, a mechanistic modelling approach is required to identify source-water controls. This was confirmed by uniformly weak and non-significant Pearson correlations between root cellulose $\delta^{18}O$ and all six candidate source waters across both datasets, whether assessed at sample level or aggregated to site means (all $r < 0.26$, all $p > 0.11$, Table S5). The model (Sect. 2.5) was therefore applied to each of the five candidate source waters in turn. Although precipitation and root-associated water are external or upstream pools rather than direct source waters for cellulose synthesis, they are included here to establish a performance baseline and to provide continuity with the pilot study (Amesbury et al., 2015a), in which root-associated water was the primary source-water candidate.

In the spatial dataset, isoscape precipitation and internal root water alone were the poorest-performing predictive source waters, with large negative mean offsets (-6.18 ‰ and -7.52 ‰ respectively) and fewer than 6 % of samples predicted within ± 3 ‰ (Table 4, Fig. 5). Root-associated water performed substantially better (mean offset -4.88 ‰, 35.1 % within ± 3 ‰, n = 37), consistent with the finding from Sect. 3.1.2 that this water pool captures a peatland-integrated source-water signal. Internal shoot water alone produced large positive offsets (+8.70 ‰), reflecting the isotopically enriched character of shoot waters relative to root cellulose (Tables S2-S4).

The most predictive source water in the spatial dataset was the mean of internal root and internal shoot water (for mechanistic interpretation of this result, see Sect. 4.2), which produced a near-zero mean offset (+0.59 ‰) and the highest proportion of samples within ± 3 ‰ (41.0 %, n = 39, Table 4, Fig. 5). This result directly supports hypothesis H3: that a combination of internal root and shoot water, rather than any single external or internal water pool, best predicts root cellulose $\delta^{18}O$.

The temporal dataset showed the same overall pattern. Measured precipitation and root-associated water both produced systematic negative offsets (-5.39 ‰ and -4.36 ‰, respectively), and internal root water alone was the least predictive source (mean offset -7.60 ‰, only 3.8 % within ± 3 ‰). Again, the mean of internal root and shoot water achieved the smallest mean offset (-2.26 ‰) and the highest proportion within ± 3 ‰ (34.6 %, n = 26, Table 4, Fig. 5), reinforcing the spatial finding. Although modest in absolute terms, this represents the best-performing source water in the temporal dataset by a substantial margin. The somewhat larger mean offset in the temporal dataset may in part reflect greater seasonal variability in temperature and humidity conditions at the two monitored sites (MOA and OTT), introducing additional scatter in the evaporative enrichment term.

These findings show that root cellulose $\delta^{18}O$ in *Empodisma* is best described as deriving from a mixed internal plant-water source in which both root and shoot water pools contribute to cellulose synthesis.

https://doi.org/10.5194/egusphere-2026-4962
Preprint. Discussion started: 25 August 2026

Candidate source water	Spatial dataset				Temporal dataset			
	Offset ± SD (‰)	*N within ± 3 ‰*	*% within ± 3 ‰*	*n total*	Offset ± SD (‰)	*N within ± 3 ‰*	*% within ± 3 ‰*	*n total*
Isoscape / measured precipitation	-6.18 ± 1.57	*2*	5.1	39	-5.39 ± 2.37	*5*	20.8	24
Root-associated water	-4.88 ± 3.38	*13*	35.1	37	-4.36 ± 2.10	*5*	19.2	26
Internal root water	-7.52 ± 3.51	*2*	5.1	39	-7.60 ±2.72	*1*	3.8	26
Internal shoot water	8.70 ± 9.25	*10*	25.6	39	3.28 ± 7.70	*7*	28.0	25
Mean internal root + shoot water	0.59 ± 4.78	*16*	41.0	39	-2.26 ± 4.06	*9*	34.6	26

Table 4. Mechanistic model performance for root cellulose $\delta^{18}O$ based on five candidate source waters in the spatial and temporal datasets. Values are shown for the combined Spatial and combined temporal (MOA+OTT) subsets only. Mean offset is expressed as predicted minus measured root cellulose $\delta^{18}O$ (‰), so values closest to zero indicate better model performance.

In the spatial dataset, precipitation refers to isoscape precipitation; in the temporal dataset, it refers to measured precipitation. The mechanistic model used ε_b = 27 ‰ and ε_k = 28.5 ‰, with temperature assignment following the species-based Kauri line rule: MAT for *E. robustum* and MST for *E. minus*.

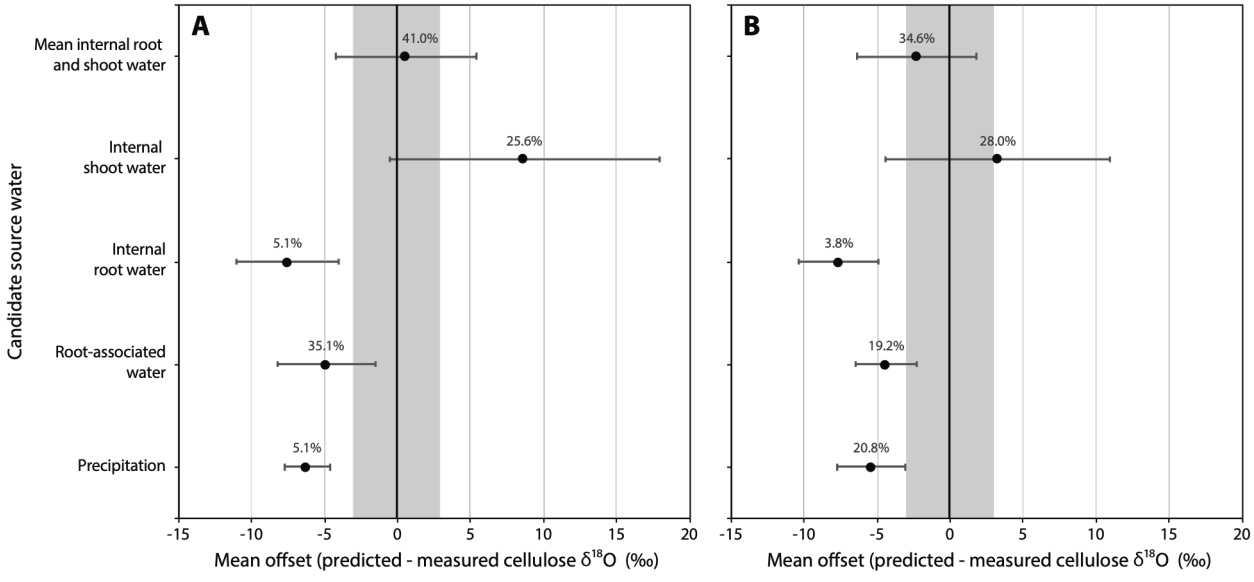

https://doi.org/10.5194/egusphere-2026-4962
Preprint. Discussion started: 25 August 2026

Figure 5. Mechanistic model performance for root cellulose $\delta^{18}O$ based on five candidate source waters in (A) the spatial dataset and (B) the combined temporal dataset (MOA+OTT). Points show the mean signed offset between model-predicted and measured root cellulose $\delta^{18}O$ (‰), and horizontal error bars show ± 1 SD. The shaded band indicates the ± 3 ‰ performance threshold. Percentages indicate the proportion of samples with predictions within the ± 3 ‰ of measured values. In the spatial dataset, precipitation refers to isoscape-modelled precipitation; in the temporal dataset, it refers to measured precipitation. The mean of internal root and internal shoot water (highlighted) performs best in both datasets, supporting H3.

3.1.5. Two-endmember mixing model

The mechanistic comparison (Sect. 3.1.4) identifies the mean of internal root and shoot water as the best-performing source water for predicting root cellulose $\delta^{18}O$. To quantify the relative contributions of these two pools, a two-endmember isotope mixing framework was applied (Eq. (4)-(5); Sect. 2.5). Three complementary model formulations were used: a fixed-ratio optimisation model as the primary result, a per-sample exact-fit model as a diagnostic supplement, and a zero-mean fixed-ratio model as a sensitivity check. The fixed-ratio optimisation minimises the mean absolute error (MAE) between predicted and measured cellulose $\delta^{18}O$ by identifying a single shared root-water fraction (f_A) across a defined group of samples. Unlike the per-sample exact-fit approach, this formulation provides a single interpretable parameter that characterises the average source-water partitioning of a population and is therefore preferred for cross-group comparisons.

3.1.5.1. Spatial dataset – global optimum

Across all spatial samples, the MAE-minimising fixed-ratio optimisation yields a global optimal f_A of 0.627 (f_B = 0.373, n = 39; Table 5, Fig. 6), indicating that root cellulose $\delta^{18}O$ is, on average, most consistent with a root-water-dominated internal source. At this optimum, the mean offset between predicted and measured cellulose $\delta^{18}O$ is -1.46 ‰ (SD = 3.90 ‰), and 43.6 % of samples are predicted within ± 3 ‰.

3.1.5.2. Species-specific partitioning

When the spatial dataset is subdivided by species, pronounced differences in optimal f_A emerge (Fig. 6). *E. robustum* sites exhibit a substantially higher root-water contribution (f_A = 0.770, 75.0 % within ± 3 ‰, n = 12), whereas *E. minus* sites show a more even partitioning, leaning towards shoot water (f_A = 0.414, 66.7 % within ± 3 ‰, n = 27). A Welch two-sample t-test on per-sample exact-fit f_A values confirms that this species difference is significant (*E. robustum*: mean = 0.751, SD = 0.087, n = 10; *E. minus*: mean = 0.421, SD = 0.186, n = 21; t = 6.73, df = 29, $p < 0.001$), a result corroborated by a non-parametric Mann-Whitney test (U = 196, $p < 0.001$). This species difference is consistent with the greater mean fractionation between root-associated and internal root water observed for *E. robustum* (3.89 ‰) relative to *E. minus* (2.46 ‰) reported in Sect. 3.1.3, and may reflect physiological differences between the two species in patterns of water uptake, internal transport, and tissue allocation.

https://doi.org/10.5194/egusphere-2026-4962
Preprint. Discussion started: 25 August 2026

3.1.5.3. Latitudinal gradient in source-water partitioning

Site-level optimal f_A also shows a positive latitudinal trend when sites are ordered from south to north (Fig. 6), with more northerly sites, all dominated by *E. robustum*, consistently returning higher root-water fractions (range 0.644-0.875) than most southern *E. minus* sites (range 0.000-0.743). A Pearson correlation between latitude and site-level MAE-optimal f_A yields r = 0.517 (p = 0.070, n = 13), which is marginally non-significant but directionally consistent with the species-driven pattern. Given the collinearity between species identity and latitude in this dataset, these two sources of variation cannot be fully separated. Nevertheless, the directional consistency of the site-level latitudinal pattern with the formally confirmed species difference (Sect. 3.1.5.2) lends additional coherence to this finding.

3.1.5.4. Temporal dataset – seasonal partitioning

In the temporal dataset, fixed-ratio optimisation reveals strong intra-annual variability in source-water partitioning at the combined site level. During the November-March (NovMar) period, the optimal f_A is 0.700, closely matching the *E. robustum*-dominated spatial result, whereas during the April-October (AprOct) period f_A falls to 0.086, indicating an overwhelming shift towards shoot-water dominance (Table 5). This pronounced seasonal contrast is primarily driven by Moanatuatua (MOA); because Otautau (OTT) exhibits comparatively stable partitioning across seasons (OTT NovMar f_A = 0.385, OTT AprOct f_A = 0.382), the combined temporal optima converge on the MOA site-specific values (MOA NovMar f_A = 0.700, MOA AprOct f_A = 0.086).

3.1.5.5. Per-sample exact-fit model (diagnostic)

The per-sample exact-fit model yielded viable solutions for 31 of 39 spatial samples and 14 of 25 temporal samples (spatial mean f_A = 0.527, SD 0.224; temporal mean f_A = 0.465, SD 0.215), broadly consistent with but somewhat lower than the primary fixed-ratio optimum (f_A = 0.627); the difference reflects the exclusion of eight non-viable samples from the per-sample mean, together with the different optimisation objectives of the two formulations. Non-viable samples are concentrated in the AprOct period, when internal root and shoot waters converge isotopically during the non-growing season, as shown by the reduced enrichment of internal shoot water in AprOct at both temporal sites (Table S3); when the two endmembers are isotopically similar, exact-fit solutions fall outside the physically meaningful [0,1] range, reflecting narrow endmember spacing rather than model failure. A zero-mean fixed ratio sensitivity check closely parallels the MAE optima and confirms that the species contrast is robust to optimisation criterion (Table S6).

https://doi.org/10.5194/egusphere-2026-4962
Preprint. Discussion started: 25 August 2026

Group	f_A (MAE)	f_B (MAE)	Mean offset (‰)	SD (‰)	n within ± 3 ‰	% within ± 3 ‰	n total
Spatial global							
All spatial samples	0.627	0.373	-1.46	3.90	17	43.6	39
Spatial by species							
E. robustum	0.770	0.230	-1.08	2.54	9	75.0	12
E. minus	0.414	0.586	-0.45	3.12	18	66.7	27
Temporal, combined seasonal							
NovMar (combined)	0.700	0.300	-2.85	3.10	5	41.7	12
AprOct (combined)	0.086	0.914	-1.59	4.32	4	30.8	13
Temporal, site and season							
MOA NovMar	0.700	0.300	-1.60	3.44	4	66.7	6
MOA AprOct	0.086	0.914	-2.01	2.61	4	57.1	7
OTT NovMar	0.385	0.615	-0.50	3.54	3	50.0	6
OTT AprOct	0.382	0.618	-3.10	3.80	1	16.7	6

Table 5. Fixed-ratio two-endmember mixing model results based on mean absolute error (MAE) optimisation. Values are shown for the spatial global dataset, spatial species groups, combined temporal season groups, and temporal site x season subsets. f_A represents the optimal fraction of internal root water and $f_B = 1 - f_A$ the corresponding fraction of internal shoot water. Mean offset is expressed as predicted minus measured cellulose $\delta^{18}O$ (‰). Lower absolute mean offsets and higher percentages within ± 3 ‰ indicate better model performance.

https://doi.org/10.5194/egusphere-2026-4962
Preprint. Discussion started: 25 August 2026

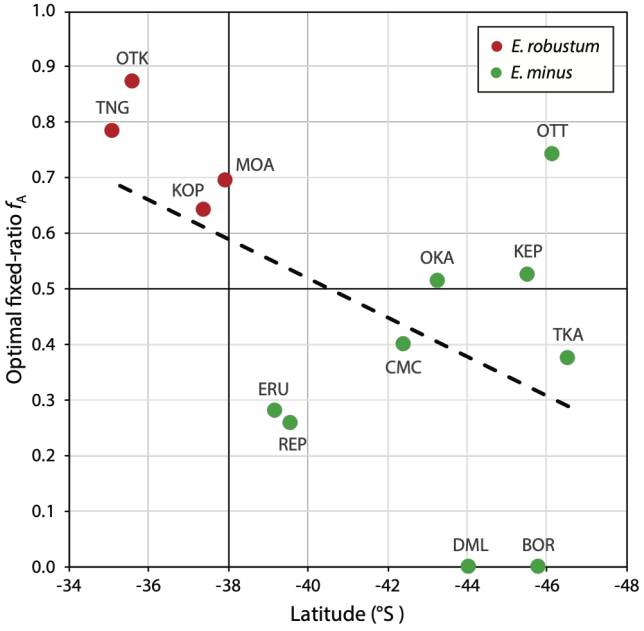

Figure 6. Site-level optimal root-water fraction (f_A) from the MAE-minimising fixed-ratio mixing model plotted against latitude. Points are coloured by species: *E. robustum* and *E. minus*; site codes labelled. The dashed line shows the overall linear trend, the solid horizontal line marks $f_A = 0.5$, and the solid vertical line marks the Kauri line (~38° S). Sites BOR and DML return $f_A \approx 0$; interpretation of this result is discussed in Sect. 4.2. The positive latitudinal relationship (r = 0.517, p = 0.070) is driven largely by the species contrast, with *E. robustum* sites returning consistently higher root-water fractions than *E. minus* sites.

Overall, this indicates that root cellulose $\delta^{18}O$ in *Empodisma* integrates a mixed plant-water signal in which internal root water is, on average, the dominant but not exclusive contributor. The magnitude of root-water dominance varies systematically with species identity, and to a lesser degree with season, providing a basis for interpreting the sources of $\delta^{18}O$ variability in downcore records from sites dominated by either species.

3.2. Carbon isotopes

3.2.1 Spatial patterns in cellulose $\delta^{13}C$

All analyses use a combined carbon dataset comprising previously published measurements (Amesbury et al., 2015b) and new data generated in this study, excluding Erua (ERU) and Crooked Mary Creek (CMC) on the basis of suspected groundwater influence on peatland waters at those sites (n = 12 for site-mean analyses; n = 69 samples for sample-level analyses).

Site-mean root cellulose $\delta^{13}C$ values become progressively less negative towards higher southern latitudes, yielding a significant positive latitudinal trend (R^2 = 0.33; Fig. 7). This gradient is evident across both northern and southern site

https://doi.org/10.5194/egusphere-2026-4962
Preprint. Discussion started: 25 August 2026

groupings and persists when within-site variability is accounted for using standard errors derived from replicate measurements.

A distinct inflection in the latitudinal distribution occurs close to ~38° S, coincident with the Kauri line (Fig. 7). Sites north of this boundary tend to exhibit more negative $\delta^{13}C$ values (more isotopically depleted cellulose), whereas sites to the south show comparatively enriched values, although substantial within-region variability remains. This biogeographic boundary also marks the transition between *Empodisma robustum* to the north and *E. minus* to the south (Wagstaff and Clarkson, 2012). A species effect on $\delta^{13}C$ is apparent in the data: mean site-level root cellulose $\delta^{13}C$ is -26.56 ‰ for *E. robustum* sites and -25.72 ‰ for *E. minus* sites, a difference that is statistically significant (Welch t-test: t = -2.92, p = 0.016; Table 6). Shoot cellulose shows a similar and somewhat stronger species contrast (-25.65 ‰ versus -24.30 ‰; t = -4.25, p = 0.003). Species identity, latitude and growing-season length are mutually collinear in this dataset – *E. robustum* sites in the north grow year-round whereas *E. minus* sites in the south have a shorter, summer-restricted growing season (Sect. 2.5) – so these two sources of variation cannot be fully separated, and the species contrast likely reflects in part the underlying climatic gradient along the transect. These spatial trends indicate that cellulose $\delta^{13}C$ integrates broad-scale environmental gradients, motivating further examination of specific climatic drivers.

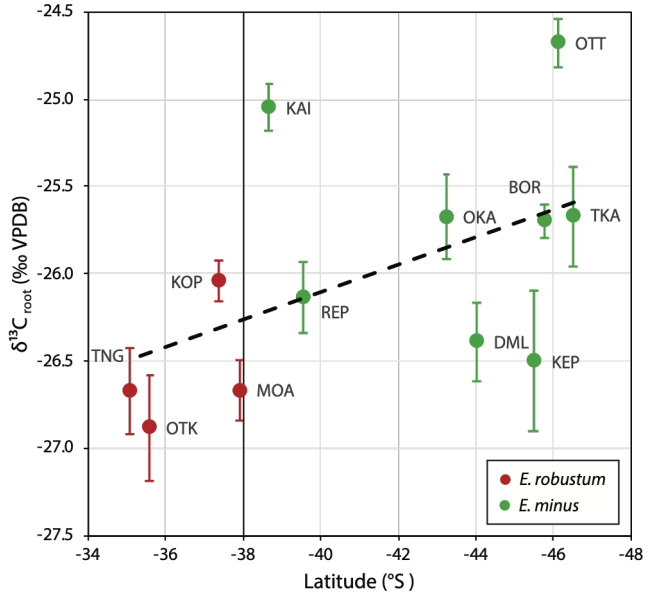

Figure 7. Latitudinal variation in mean root cellulose $\delta^{13}C$ across the Aotearoa New Zealand peatland transect. Points show site means with error bars representing ±1 standard error. Site labels correspond to peatland locations. The solid vertical line marks the approximate position of the Kauri line (~38° S), separating the northern distribution of *Empodisma robustum* from the southern distribution of *E. minus*. The dashed line shows the fitted linear regression ($R^2 = 0.33$) across all sites.

https://doi.org/10.5194/egusphere-2026-4962
Preprint. Discussion started: 25 August 2026

Tissue	*E. robustum* mean ± SD (n)	*E. minus* mean ± SD (n)	Welch t	p	df
Root cellulose	-26.56 ± 0.36 (4)	-25.72 ± 0.63 (8)	-2.92	0.016	9.53
Shoot cellulose	-25.65 ± 0.48 (4)	-24.30 ± 0.59 (8)	-4.25	0.003	7.40

Table 6. Species comparison of site-mean cellulose $\delta^{13}C$ values (‰ VPDB) using Welch two-sample t-tests. Values are means ± SD. Groundwater-influenced sites ERU and CMC were excluded.

3.2.2. Root versus shoot $\delta^{13}C$

Root and shoot cellulose $\delta^{13}C$ values are strongly positively correlated across sites (Fig. 8), indicating that both tissues record a broadly coherent isotopic signal. A linear regression of site-mean shoot $\delta^{13}C$ yields $R^2 = 0.68$ ($p < 0.001$, $n = 12$). However, shoot cellulose is systematically enriched relative to root cellulose across all sites, with a mean offset of +1.25 ‰ (shoot minus root; paired t-test: $t = 9.01$, $p < 0.001$, $n = 12$). All paired measurements plot above the 1:1 line, confirming this enrichment is consistent and not driven by a small number of sites.

The strength of the root-shoot relationship demonstrates that variation in $\delta^{13}C$ is shared between tissues, supporting the use of root cellulose as a reliable archive of site-level carbon isotope signals. The systematic shoot enrichment is noted here as an empirical observation, and its physiological basis is considered further in the Discussion.

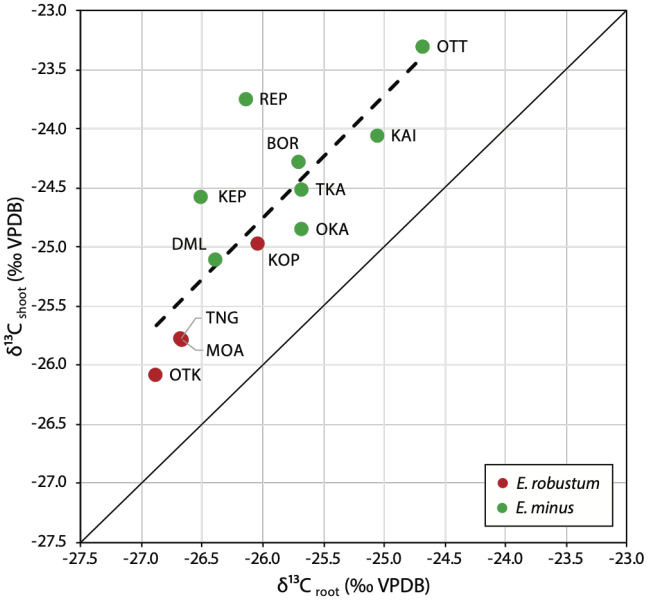

Figure 8. Relationship between site-mean root and shoot cellulose $\delta^{13}C$ for 12 Aotearoa New Zealand peatland sites. Points are coloured by species and labelled by site code. The solid line shows the 1:1 relationship and the dashed line the fitted regression. Root and shoot $\delta^{13}C$ are strongly positively correlated ($R^2 = 0.68$, $p < 0.001$), but shoot cellulose is consistently enriched relative to root cellulose by a mean of +1.25‰.

https://doi.org/10.5194/egusphere-2026-4962
Preprint. Discussion started: 25 August 2026

3.2.3. Cellulose $\delta^{13}C$ and temperature and energy variables

Correlation statistics between site-mean cellulose $\delta^{13}C$ and climate variables are summarised in Table 7. Strong and consistent negative relationships are observed between cellulose $\delta^{13}C$ and variables describing thermal regime and energy availability (Fig. 9). For both roots and shoots, $\delta^{13}C$ becomes progressively more negative with increasing MAT and MST, indicating isotopically depleted cellulose at warmer, more energy-rich sites. These relationships are significant for both tissue types (root vs MAT: $r = -0.613$, $p = 0.034$; root vs MST: $r = -0.628$, $p = 0.029$; shoot vs MAT: $r = -0.852$, $p < 0.001$; shoot vs MST: $r = -0.820$, $p = 0.001$; all $n = 12$), and are stronger for shoot than root cellulose, though the direction is consistent.

Photosynthetically active radiation (PAR_0) and growing degree days above 0°C (GDD_0) show negative trends in the same direction, with more negative $\delta^{13}C$ at higher-energy sites, although these relationships are weaker and do not reach conventional significance thresholds for root cellulose (root vs PAR_0: $r = -0.433$, $p = 0.160$; root vs GDD_0: $r = -0.471$, $p = 0.122$). For shoots, PAR_0 approaches significance ($r = -0.575$, $p = 0.050$). The consistency of direction across all four energy-related variables strengthens the overall inference that thermal and energy regime exerts a first-order control on cellulose carbon isotopic composition across the Aotearoa New Zealand peatland transect.

The negative direction of these relationships is consistent with the carbon isotope discrimination framework (Farquhar et al., 1989), now confirmed with greater statistical power and spatial extent across 12 sites spanning more than 11° of latitude. A supplementary analysis restricted to the newly sampled sites (n=11, i.e. groundwater-influenced ERU and CMC are excluded throughout, and KAI was not resampled in this study) confirms the robustness of the temperature signal for shoot cellulose ($r = -0.843$, $p = 0.001$) and yields a directionally consistent but marginally non-significant result for roots ($r = -0.586$, $p = 0.058$), attributable to reduced statistical power, as KAI was not resampled in this study and so does not contribute to the temperature correlations. In contrast, all relationships between $\delta^{13}C$ and moisture variables are weak and non-significant for both tissues (Table 7; Fig. 10; all $p > 0.10$), confirming that carbon isotope discrimination is governed primarily by thermal regime rather than water deficit across the range of conditions sampled (Amesbury et al., 2015b).

https://doi.org/10.5194/egusphere-2026-4962
Preprint. Discussion started: 25 August 2026

Climate variable	Root cellulose			Shoot cellulose		
	r	p	n	r	p	n
Mean annual temperature (MAT)	**-0.613***	0.034	12	**-0.852****	<0.001	12
Mean summer temperature (MST)	**-0.628***	0.029	12	**-0.820****	0.001	12
PAR_0	-0.433	0.160	12	-0.575	0.050	12
GDD_0	-0.471	0.122	12	-0.484	0.111	12
Mean annual precipitation (MAP)	0.039	0.903	12	-0.102	0.752	12
Mean summer precipitation (MSP)	0.051	0.874	12	-0.054	0.869	12
Relative humidity (RH)	-0.183	0.570	12	-0.485	0.110	12
Moisture index (MI)	0.408	0.188	12	0.178	0.581	12
Soil moisture	0.345	0.272	12	0.256	0.422	12

695

Table 7. Pearson correlations between site-mean cellulose $\delta^{13}C$ and climate variables across 12 Aotearoa New Zealand peatland sites. Values shown are Pearson's r, p, and n. Bold values indicate statistically significant Pearson correlation coefficients; * $p < 0.05$, ** $p < 0.01$. Groundwater-influenced sites ERU and CMC were excluded.

https://doi.org/10.5194/egusphere-2026-4962
Preprint. Discussion started: 25 August 2026

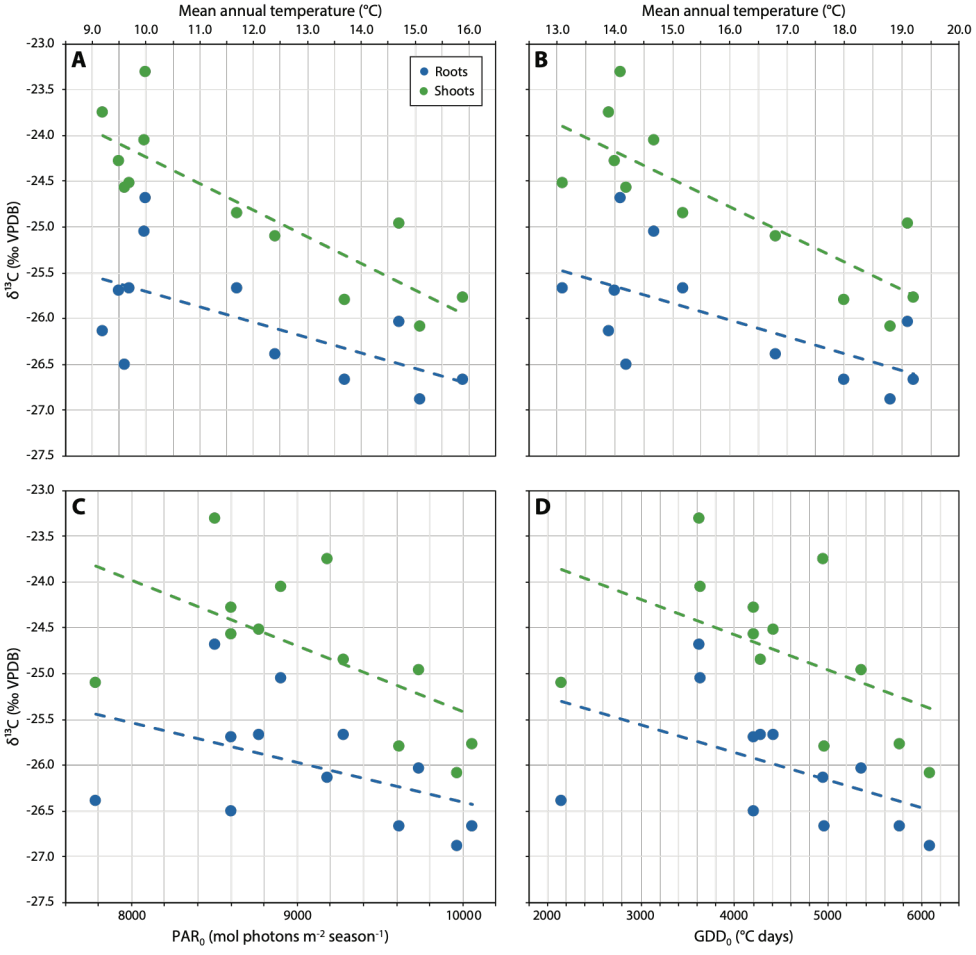

Figure 9. Relationships between site-mean cellulose $\delta^{13}C$ and temperature/energy variables across 12 Aotearoa New Zealand peatland sites. Panels show (A) mean annual temperature (MAT), (B) mean summer temperatures (MST), (C) cumulative photosynthetically active radiation during the growing seasons (PAR_0), and (D) growing degree days above 0°C (GDD_0). Points and fitted lines are shown separately for root and shoot cellulose. For both tissues, $\delta^{13}C$ becomes more negative with increasing temperature and energy availability, with the strongest relationships for MAT and MST.

https://doi.org/10.5194/egusphere-2026-4962
Preprint. Discussion started: 25 August 2026

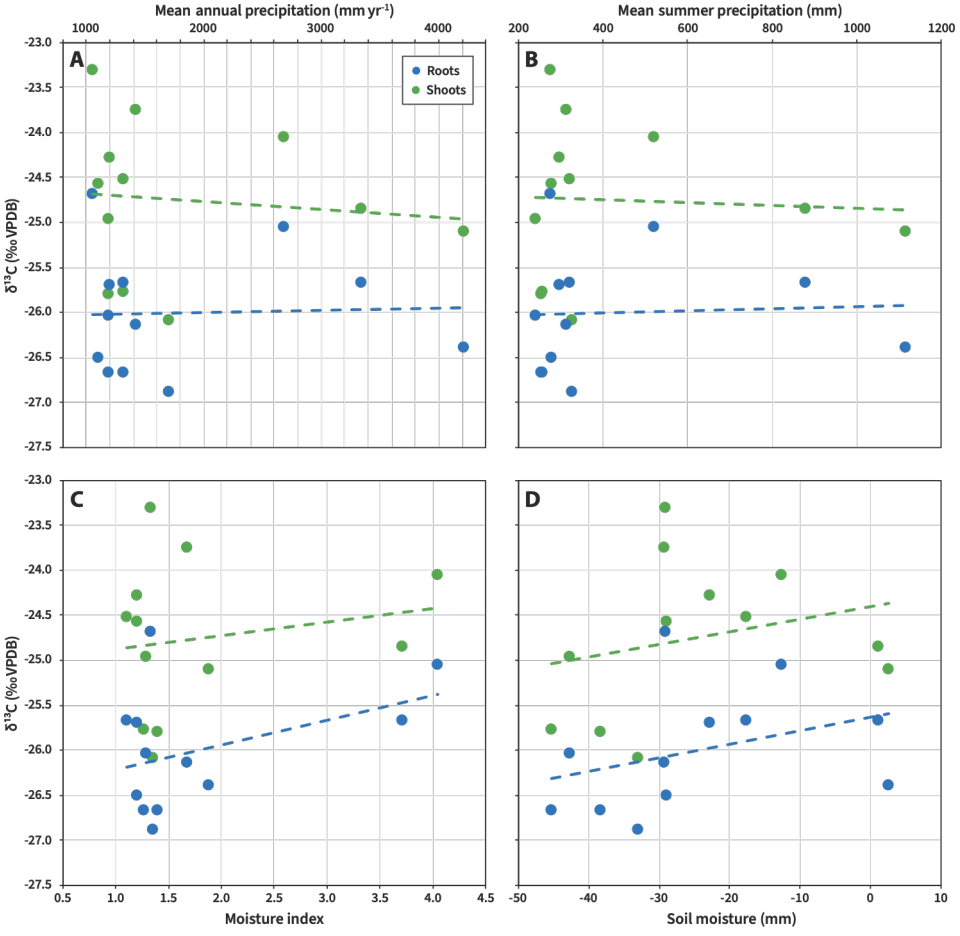

Figure 10. Relationships between site-mean cellulose $\delta^{13}C$ and moisture variables across 12 Aotearoa New Zealand peatland sites. Panels show (A) mean annual precipitation (MAP), (B) mean summer precipitation (MSP), (C) moisture index (MI), and (D) modelled soil moisture. Points and fitted lines are shown separately for root and shoot cellulose. In contrast to the temperature/energy variables, relationships with moisture metrics are weak and non-significant for both tissues.

3.2.4. $\delta^{13}C$ and water table depth

Although site-mean moisture indices show no significant relationship with cellulose $\delta^{13}C$, sample-level analysis reveals a modest but statistically significant association between root cellulose $\delta^{13}C$ and water table depth (WTD) (Fig. 11). Root cellulose $\delta^{13}C$ becomes progressively more negative under drier microhabitat conditions (i.e. at greater WTD) with a linear regression explaining 27 % of the among-sample variance ($R^2 = 0.272$, slope = -0.021 ‰ cm^{-1}, $p < 0.001$, $n = 69$). A weaker but still significant relationship is observed for shoot cellulose ($R^2 = 0.119$, slope = -0.016 ‰ cm^{-1}, $p = 0.004$, $n = 69$).

This relationship runs opposite to the enrichment expected from stomatal closure under water deficit, and is consistent with the earlier finding that *Empodisma* is not water-stressed under normal conditions (Amesbury et al., 2015b). In the pilot

https://doi.org/10.5194/egusphere-2026-4962
Preprint. Discussion started: 25 August 2026

dataset the equivalent relationship could not be separated from the influence of MOA and TNG, where drainage of surrounding agricultural land has lowered water tables, because their removal left too narrow a range of water-table depths to test (Amesbury et al., 2015b). The addition of REP, an unmodified site with among the deepest water tables in the dataset, now allows that test: across sites other than MOA and TNG the sampled range remains close to that of the full dataset, and the relationship persists with a similar slope (R^2 = 0.120, slope = -0.016 ‰ cm^{-1}, p = 0.013, n = 51). Nor is it an expression of the latitudinal gradient: partitioning the variance shows the relationship is stronger within sites (R^2 = 0.123, p = 0.003) than between site means (R^2 = 0.255, p = 0.094). Possible mechanisms include greater assimilation of ^{13}C-depleted respired CO_2 within a thicker aerated peat profile, or relief of the constraints imposed on cluster-root function by waterlogging, but these data do not distinguish between them. The effect is modest relative to the temperature and energy controls identified at the site scale, and substantial scatter remains within individual sites. The WTD effect therefore represents a secondary, within-site source of $\delta^{13}C$ variability rather than a primary driver of the larger-scale spatial gradient.

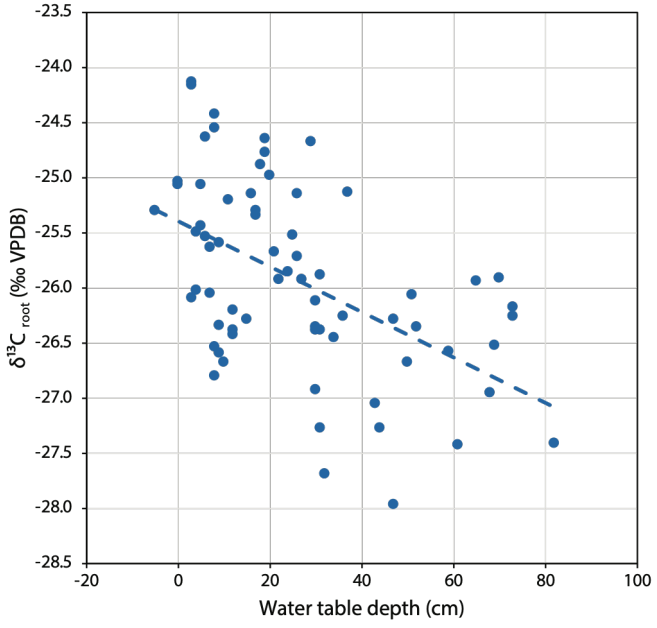

Figure 11. Relationship between sample-level root cellulose $\delta^{13}C$ and water table depth (WTD) for the combined carbon dataset, including previously published data and new measurements from this study**.** Points therefore represent individual samples from 12 sites after exclusion of Erua (ERU) and Crooked Mary Creek (CMC). The dashed line shows the fitted linear regression. Root cellulose $\delta^{13}C$ becomes more negative at greater WTD, with the regression explaining 27 % of the among-sample variance (R^2 = 0.272, slope = -0.021 ‰ cm^{-1}, p < 0.001, n = 69).

https://doi.org/10.5194/egusphere-2026-4962
Preprint. Discussion started: 25 August 2026

3.3. Pilot palaeo-application

3.3.1. Downcore isotope stratigraphy

Root cellulose $\delta^{18}O$ and $\delta^{13}C$ records are presented for Tangonge (TNG, North Island, ~ 35° S, *E. robustum*) and Otautau (OTT; South Island, ~46° S, *E. minus*) from approximately 1900 CE to the present day (Fig. 12). The TNG record comprises contiguous 1-cm sampling to 31 cm depth, and OTT comprises contiguous 1-cm sampling to 41 cm depth, followed by non-contiguous 1-cm sampling thereafter. Chronological control is provided by combined ^{210}Pb and ^{14}C Bayesian age-depth models (Sect. 2.6, Fig. S1), with mean per-sample age uncertainty of approximately ± 6 years at TNG and ± 5 years at OTT. Individual sample age ranges are small and fairly uniform throughout both records, reflecting good chronological constraint in the near-surface peat.

At TNG, root cellulose $\delta^{18}O$ values range from 30.84 to 34.79 ‰ across the record, with a pre-1970 mean of 32.58 ‰ increasing to a post-1970 mean of 33.29 ‰ (Fig. 12A). Loess smoothing shows a broadly stable or slightly declining trajectory from approximately 1900 to 1960, followed by a trend towards more enriched values through the latter half of the 20th century, with particularly enriched values in the most recent decade (33.5-34.8 ‰). Measured root cellulose $\delta^{13}C$ at TNG ranges from -29.01 to -26.93 ‰ (Fig. 12C). Here, loess smoothing shows values centred around -28 ‰ through most of the first three quarters of the record, with the most depleted measured value in the record (-29.01 ‰) occurring around 1973 CE (± 2.4 years) before a general trend towards less negative values in recent decades, with the most recent samples spanning -28.24 to -27.04 ‰. The measured pre-1970 mean of -28.05 ‰ compares to a post-1970 mean of -27.84 ‰, an apparent enrichment of only +0.21 ‰. Both means are depressed by the industrial-period decline in atmospheric $\delta^{13}C$-CO_2; after correction for the Suess effect the same comparison gives -27.73 ‰ and -26.45 ‰, an enrichment of +1.28 ‰ (Fig. 12C).

At OTT, root cellulose $\delta^{18}O$ values range from 28.58 to 34.92 ‰ and are systematically lower than at TNG for much of the early record, consistent with the more depleted isoscape precipitation at this high-latitude South Island site (Fig. 12B; Table 1). Loess smoothing reveals a pronounced trend: values are relatively stable and low through the early-to-mid 20th century (pre-1970 mean 30.66 ‰) before rising substantially, with post-1970 values averaging 32.00 ‰ and the most recent samples reaching 33.97-34.92 ‰; an enrichment of approximately 3-4 ‰ between the early record and the present. Measured root cellulose $\delta^{13}C$ at OTT ranges from -26.99 to -24.93 ‰, systematically less negative than TNG throughout the record, consistent with the *E. minus* species baseline established in the surface calibration (Fig. 12D; Sect. 3.2.1). Loess smoothing of the measured values shows relatively stable values around -25.5 to -26 ‰ through most of the 20th century, with no strong depletion excursion in the 1970s and a slight net depletion of -0.15 ‰ between the pre- and post-1970 means. This apparent stability is an expression of the atmospheric trend rather than of the plant signal: after Suess correction the record enriches from -25.29 ‰ to -24.44 ‰ across the same boundary, an increase of +0.85 ‰ (Fig. 12D), in the same direction as TNG.

https://doi.org/10.5194/egusphere-2026-4962
Preprint. Discussion started: 25 August 2026

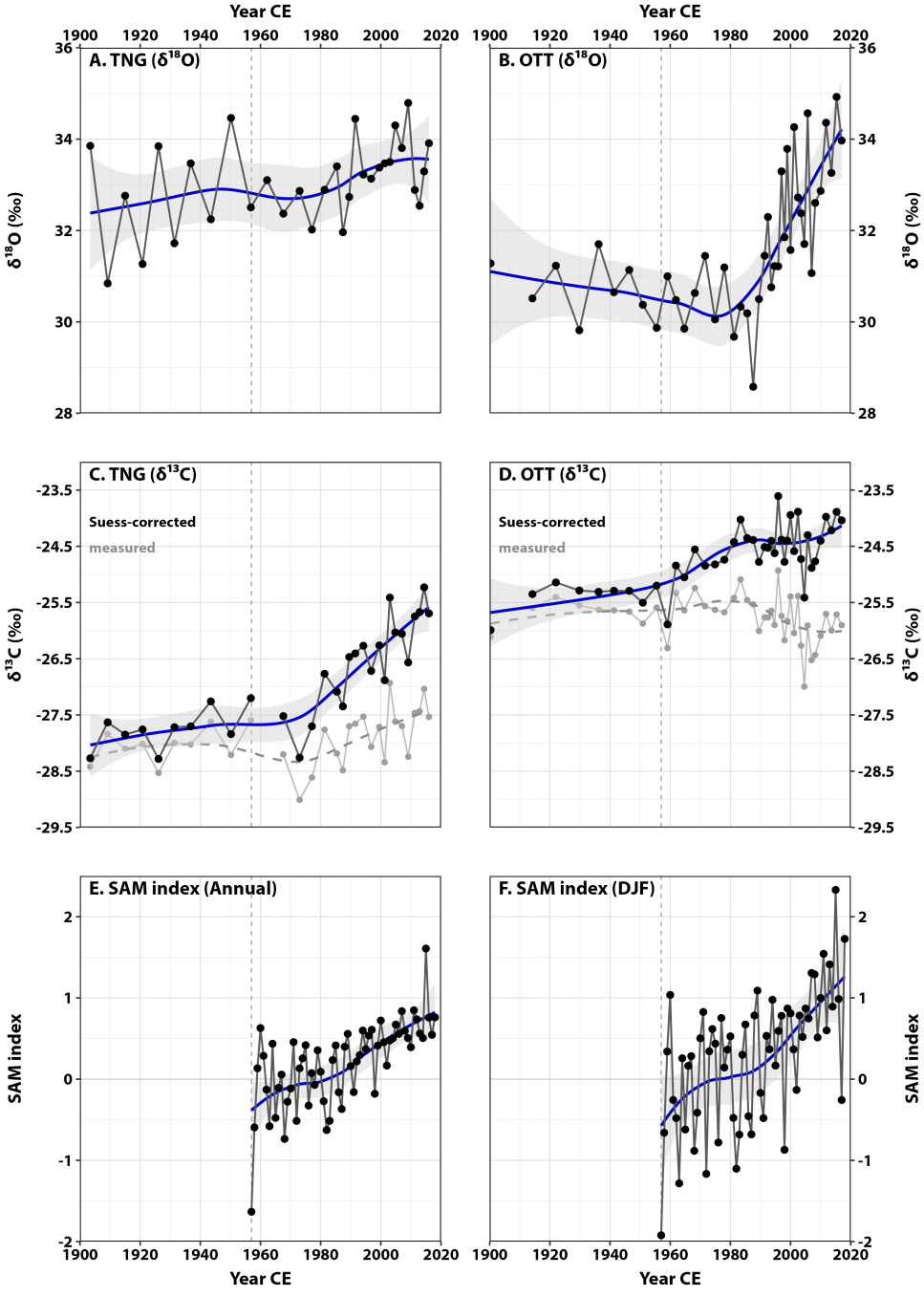

Figure 12. Down-core root cellulose $\delta^{18}O$ and $\delta^{13}C$ records from Tangonge (TNG, North Island, ~35° S, *Empodisma robustum*; panels A and C) and Otautau (OTT, South Island, ~46° S, *E. minus*, panels B and D) spanning 1900 CE to the present day, plotted against (E) annual and (F) summer (DJF) mean SAM index series. Panels C and D show downcore $\delta^{13}C$ as measured (grey) and after correction for

https://doi.org/10.5194/egusphere-2026-4962
Preprint. Discussion started: 25 August 2026

the atmospheric Suess effect (black), following Graven et al. (2017). The correction removes the industrial-period decline in atmospheric $\delta^{13}C$-CO_2 and is required for comparison of pre- and post-industrial values; measured values are retained to show the magnitude of the adjustment. Blue lines are loess smoothers (span = 0.75) with grey shaded 95 % confidence envelopes; in panels C and D the smoother is fitted to the corrected series and the grey dashed line to the measured series. The vertical dotted line marks the start of the instrumental SAM index in 1957. Within each row, both panels share a common y-axis range so that the amplitude of variability is directly comparable between the two sites.

3.3.2. Comparison with the SAM index

The SAM index (Marshall, 2003) shows a well-documented positive trend over the instrumental period (Fig. 12E-F), with values transitioning from near-neutral or weakly negative in the mid-20th century to persistently positive from approximately the 1970s-1980s onwards. This trend is more pronounced in the DJF seasonal mean (Fig. 12F) than in the annual mean (Fig. 12E), consistent with the strong austral summer expression of SAM-related climate variability over Aotearoa New Zealand (Kidston et al., 2009).

As established in Sect. 3.1.1, the isotopic expression of SAM variability over Aotearoa New Zealand is determined primarily by its effect on moisture source provenance rather than a simple latitudinal shift of the westerly wind belt. The IsoGSM composites (Fig. 2) confirm that SAM-related isotopic contrasts are strongest over the North Island during DJF, with weaker and more spatially variable anomalies over the far south of the South Island, making TNG, a priori, the more sensitive SAM $\delta^{18}O$ recorder of the two sites. This expectation applies primarily to the summer precipitation signal; annual downcore cellulose $\delta^{18}O$ may integrate a broader seasonal window and additional site-specific plant-water effects, potentially allowing OTT to show a larger annual-amplitude response despite weaker DJF sensitivity.

For the carbon isotope records, the surface calibration predicts that positive SAM should drive $\delta^{13}C$ towards more negative (depleted) values at both sites, via the associated warmer and more settled summer conditions promoting greater stomatal conductance and enhanced carbon isotope discrimination (Sect. 3.2.3; Farquhar et al., 1989).

$\delta^{18}O$ records: Both sites show enrichment in $\delta^{18}O$ over the 20th century, most clearly from approximately 1960-1970 onwards. At OTT the enrichment is substantially larger in magnitude (3-4 ‰) than at TNG (0.7 ‰ comparing pre- and post-1970 means). This enrichment trend is not straightforwardly consistent with the moisture-source framework established in Sect. 3.1.1, which would predict depleted, not enriched, $\delta^{18}O$ under a positive SAM trend at both sites. The directionality is therefore ambiguous with respect to SAM attribution. However, three factors are relevant. First, coupled enrichment in both $\delta^{13}C$ and $\delta^{18}O$ over the industrial period is the direction that would be expected from rising atmospheric CO_2 concentration: reduced stomatal conductance at a given assimilation rate increases intrinsic water-use efficiency, which reduces discrimination against ^{13}C and is expected to influence cellulose $\delta^{18}O$ through its effect on leaf water enrichment, although the magnitude of that effect is not constrained by our data. This temporal mechanism is not in conflict with the absence of spatial moisture signal in the modern calibration (Sect. 3.2.3): the spatial result shows that Empodisma $\delta^{13}C$ does not track site water availability, whereas the industrial-period trend reflects a change in atmospheric CO_2 acting on stomatal

https://doi.org/10.5194/egusphere-2026-4962
Preprint. Discussion started: 25 August 2026

conductance independently of local water status. Second, the 1976-1977 Interdecadal Pacific Oscillation (IPO) phase shift was associated with well-documented changes in Aotearoa New Zealand circulation and precipitation, and with broader regional temperature changes (Salinger et al., 2001) that are not separable from the SAM trend at this record length, and the IPO's isotopic expression in Aotearoa New Zealand precipitation is less well characterised than that of the SAM. Third, the OTT $\delta^{18}O$ enrichment trend may also reflect broader late-20th century warming of Aotearoa New Zealand and surrounding oceanic conditions, potentially affecting the isotopic composition of moisture reaching both sites regardless of trajectory. The greater magnitude of enrichment at OTT relative to TNG is of interest. The IsoGSM annual composites (Fig. 2C-D) do indicate a stronger isotopic response to SAM phase changes at OTT'S latitude on an annual basis than in DJF alone, but that modelled response is towards depletion under positive SAM, whereas the observed trend is towards enrichment; the magnitude of the OTT signal therefore cannot be attributed to SAM sensitivity. A more direct explanation follows from the mixing model. OTT lies in inland western Southland, near the southern coast of the South Island, and is dominated by *E. minus*, which has a low root-water fraction (f_A = 0.414 for the species group, against 0.770 for *E. robustum*), so its cellulose $\delta^{18}O$ is weighted towards internal shoot water, the pool most susceptible to evaporative enrichment. TNG, dominated by *E. robustum*, is more directly coupled to source water. The four- to five-fold difference in $\delta^{18}O$ amplitude between the two sites therefore tracks the species-dependent source-water partitioning established in Sect. 3.2.2, and cannot be produced by a spatially uniform forcing.

$\delta^{13}C$ records: The TNG $\delta^{13}C$ record is characterised by substantial high-frequency variability superimposed on a modest multi-decadal trend. In the measured record the most recent decade of samples (2009-2016) spans -28.24 ‰ to -27.04 ‰ against a record median of -27.92 ‰, and the post-1970 mean (-27.84 ‰) is only slightly less negative than the pre-1970 mean (-28.05 ‰). This apparent stability is misleading. Once the atmospheric Suess effect is removed (Fig. 12C), the record enriches by +1.28 ‰ across the same boundary and the five most recent samples sit between the 60th and 97th percentile of the corrected series, which is opposite in direction to the warming-driven depletion predicted by the site-scale temperature calibration. At OTT, the measured $\delta^{13}C$ record shows no clear directional trend over the 20th century, with values fluctuating around -25.5 to -26 ‰ throughout and a slight net depletion of -0.15 ‰ across the 1970 boundary. As at TNG, this is an artefact of the atmospheric trend: after Suess correction the record enriches by +0.85 ‰ (Fig. 12D). Both sites therefore enrich over the industrial period, opposite in direction to the depletion that warming-driven discrimination would predict, and the absence of a resolvable temperature signal cannot be attributed to the weaker southern temperature gradient or to WTD change (Sect. 3.2.4) alone.

3.3.3. Interpretation relative to the modern calibration framework

The pilot palaeo-application provides partial support for hypothesis H4, but with important caveats that reflect both the complexity of the Aotearoa New Zealand climate system and the inherent limitations of a 120-year record.

The most consistent signal is the coherent 20th-century enrichment in $\delta^{18}O$ at both sites, particularly the pronounced and well-resolved trend at OTT. That both proxies shift in the same direction at both sites, monotonically and over the industrial

https://doi.org/10.5194/egusphere-2026-4962
Preprint. Discussion started: 25 August 2026

period, points to a driver acting uniformly across the region – most plausibly the industrial-period rise in atmospheric CO_2 – rather than to SAM-related circulation change, whose isotopic expression differs between the two sites and would predict depletion rather than enrichment. The markedly larger $\delta^{18}O$ amplitude at OTT than at TNG is nonetheless consistent with the species-dependent source-water partitioning established in Sect. 3.2.2, indicating that the calibrated plant-water pathway is expressed in the downcore records even where the climatic driver is not resolved.

The $\delta^{13}C$ records exhibit coherent behaviour after correction for the atmospheric Suess effect. Both sites enrich between the pre- and post-1970 periods, by +1.28 ‰ at TNG and +0.85 ‰ at OTT, and in measured records this signal is masked, and at OTT slightly reversed, by the industrial-period decline in atmospheric $\delta^{13}C$-CO_2. The direction of change at both sites is opposite to the depletion predicted by the temperature calibration and matches the direction of the $\delta^{18}O$ records, consistent with a single driver acting on both proxies at both sites. High-frequency variability remains substantial at both sites, and at TNG exceeds the multi-decadal signal in the measured record.

Overall, the results show that the *Empodisma* cellulose isotope system records coherent, well-dated, multi-decadal signals in both proxies at both sites, and that the relative amplitude of the $\delta^{18}O$ signals follows the species-dependent partitioning established in Sect. 3.1 and 3.2. The direction of change in both proxies is not, however, what the SAM framework predicts, and over an interval dominated by rising atmospheric CO_2 the climatic component cannot be isolated. The records are presented here as an initial test of whether archived cellulose yields reproducible isotope signals over the instrumental period, providing a foundation for extending these records through the full Holocene. A definitive test of H4, and quantitative SAM attribution, will require longer records, multi-proxy comparison, and climate model-based attribution to separate SAM, IPO, and greenhouse warming contributions over the 20th century.

4. Discussion

4.1. The oxygen isotope pathway from precipitation to cellulose in *Empodisma* peatlands

The results presented here confirm and substantially extend the isotopic pathway framework established in the earlier study (Amesbury et al., 2015a). Precipitation $\delta^{18}O$ varies predictably along the Aotearoa New Zealand latitudinal transect, controlled primarily by moisture source provenance; the alternation between subtropical and sub-Antarctic air masses modulated by the SAM and ENSO (Baisden et al., 2016; Ummenhofer and England, 2007), and this gradient is broadly preserved in peatland waters. The close alignment of all measured peatland water pools with the global meteoric water line confirms that evaporative modification at the peatland scale is minimal across all 13 sites, extending the spatial scope of this finding well beyond the six-site pilot dataset.

The principal advance on Amesbury et al. (2015a) in the present study comes from cryogenic vacuum distillation of internal plant waters, which were not available in the earlier study. These data reveal a systematic and species-dependent offset between root-associated and internal root water (mean $\delta^{18}O$ offset 2.98 ‰; *E. robustum* 3.89 ‰ vs *E. minus* 2.46 ‰, $p = 0.033$), confirming hypothesis H2. The strong positive relationship between root-associated and internal root water ($r =$

https://doi.org/10.5194/egusphere-2026-4962
Preprint. Discussion started: 25 August 2026

0.719, $p < 0.001$, $n = 63$) demonstrates that they are closely coupled, but the systematic offset makes clear that root-associated water, which was used as a proxy for functional source water in the pilot study, does not directly represent the water pool incorporated into cellulose. The fractionation between these pools is consistent with isotopic modification between external and internal plant-water pools, likely involving internal transport and related fractionation processes within the plant, although the precise mechanisms remain less well characterised for peatland restiads specifically.

The finding that spatial precipitation-to-water transfer is weaker for root-associated water ($r = 0.35$, ns) than for bog water ($r = 0.72$, $p = 0.005$), while the temporal relationship is strong ($r = 0.79$, $p < 0.001$), reflects the different timescales of isotopic integration in these water pools. Bog water likely integrates precipitation over extended periods and tracks isoscape precipitation well spatially, whereas root-associated water integrates over shorter timescales: its weaker spatial relationship reflects local hydrological and storm-path variability not captured by the isoscape. The temporal dataset, sampling monthly within a single year, resolves the event-scale dynamics the spatial isoscape averages over, explaining the stronger temporal relationship. This is consistent with evidence that local hydrology and short-term evaporative conditions modify precipitation signals transfer into peatland waters and cellulose (Jones et al., 2019; Loader et al., 2016).

4.2. Internal plant water dynamics as the key filter on cellulose $\delta^{18}O$

The uniform absence of significant correlations between root cellulose $\delta^{18}O$ and any candidate source water ($r < 0.26$ for all pools at all levels of aggregation), as also previously noted (Amesbury et al., 2015a), confirms that simple linear relationships cannot identify source-water controls. This is expected from first principles: cellulose $\delta^{18}O$ integrates source-water composition and temperature- and humidity-dependent fractionation during evaporative enrichment and biosynthesis (Barbour, 2007; Roden et al., 2000), making mechanistic modelling a prerequisite for meaningful interpretation rather than an optional refinement.

The mechanistic model comparison directly tests hypothesis H3. The unweighted mean of internal root and shoot water $\delta^{18}O$ is the best-performing source in both spatial (mean offset +0.59 ‰, 41.0 % within ± 3 ‰) and temporal (mean offset -2.26 ‰, 34.6 % within ± 3 ‰) datasets, substantially outperforming every water pool tested in isolation. This finding indicates that cellulose synthesis in *Empodisma* draws on water from both root and shoot tissues rather than from a single source-water pool. The physical interpretation is that sucrose, the immediate precursor of cellulose synthesis, is mobilised from both root and shoot tissues, consistent with the known bidirectional phloem transport architecture of vascular plants. We note that the mixing model treats the two internal pools as static endmembers, and that these data cannot constrain their relative turnover times. If root and shoot water are replaced at different rates, the effective contribution of each to the sucrose pool will be weighted towards the more rapidly turned-over pool, and the fitted f_A should be read as an integrated contribution over the period of cellulose synthesis rather than as an instantaneous volumetric ratio. Although mixed internal water sources have not previously been demonstrated for peatland vascular plants, species- and tissue-related offsets in peatland cellulose $\delta^{18}O$ are well documented, including consistently higher $\delta^{18}O$ values in vascular plants than in *Sphagnum* despite a shared

https://doi.org/10.5194/egusphere-2026-4962
Preprint. Discussion started: 25 August 2026

peat-water source, consistent with the influence of plant functional type and transpiration on cellulose formation (Jones et al., 2019; Sakurai et al., 2021).

The two-endmember mixing model quantifies this mixed contribution. This species difference is consistent with the larger fractionation between root-associated and internal root water observed for *E. robustum* (Sect. 3.1.3) and may reflect differences between the species in root activity, water uptake depth, or shoot canopy architecture. *Empodisma robustum*-dominated peatlands experience year-round growing conditions that support photosynthesis throughout the year (Campbell et al., 2014), whereas *E. minus*, occupying higher latitudes, likely has a more seasonally constrained growing period; these phenological differences may translate to differences in the relative metabolic activity of root versus shoot tissues during the period of cellulose synthesis and thus in the relative contribution of each tissue's internal water to the sucrose pool.

The pronounced seasonal shift in source-water partitioning at Moanatuatua (MOA: NovMar f_A = 0.700, AprOct f_A = 0.086) is a genuinely novel result for which a mechanistic explanation remains tentative. During the April-October period at this North Island site, the fixed-ratio optimum collapses to near-zero root-water contribution. One plausible mechanism is that during the cooler season, root metabolic activity decreases while shoot tissues continue some carbohydrate mobilisation, shifting the effective sucrose pool towards shoot-water isotopic composition. An alternative is that cooler soil temperatures during AprOct reduce root-water uptake fluxes, leaving shoot-derived water as the dominant contributor to internal phloem transport. The contrasting stability of the OTT seasonal result ($f_A \approx 0.385$ and 0.382 in Nov-Mar and Apr-Oct respectively) is consistent with the smaller seasonal amplitude in growing conditions at this southern, maritime site. These seasonal patterns warrant further investigation with controlled experimental work.

The sites BOR and DML present a specific interpretive challenge: their fixed-ratio optima are effectively zero ($f_A \approx 0$), yet even pure shoot water under-predicts measured cellulose $\delta^{18}O$, leaving negative mean offsets of -1.21 ‰ and -3.12 ‰ respectively. Two explanations merit consideration. First, internal shoot water at both sites is anomalously depleted (values close to 0 ‰ or negative), which may reflect genuine physiological characteristics or a sampling artefact from the cold, high-rainfall conditions at these southerly sites. Second, at temperatures well below 20°C, the biochemical fractionation factor ε_b may be larger than the 27 ‰ applied uniformly here: Sternberg and Ellsworth (2011) demonstrated experimentally that ε_b increases below 20°C, with values up to 31 ‰ at colder temperatures, and BOR (MAT 9.5°C) and DML (MAT 12.4°C) are among the coldest sites in the transect. Applying a temperature-corrected ε_b at these sites would shift predicted cellulose values upward, potentially resolving the offset. Future work should explicitly test the temperature dependence of ε_b across comparable temperature gradients.

4.3. Temperature as the primary control on *Empodisma* cellulose $\delta^{13}C$

Hypothesis H1 is confirmed for carbon isotopes: the negative relationship between $\delta^{13}C$ and temperature is replicated with substantially greater statistical power and spatial extent than the earlier study (Amesbury et al., 2015b). The combined carbon dataset, comprising previously published data and new measurements from the current study (n = 12 sites, spanning >11° latitude), yields root vs MAT r = -0.613 (p = 0.034) and shoot vs MAT r = -0.852 (p < 0.001), directionally consistent

https://doi.org/10.5194/egusphere-2026-4962
Preprint. Discussion started: 25 August 2026

with and extending the original six-site findings. The direction of the relationship, more negative $\delta^{13}C$ at warmer sites, is consistent with the Farquhar et al. (1989) framework for C3 plant carbon isotope discrimination: warmer conditions are interpreted to favour greater effective discrimination against $^{13}CO_2$ during photosynthesis, likely through higher stomatal conductance and/or photosynthetic rates, producing more depleted cellulose. Under this framework, *Empodisma* $\delta^{13}C$ in Aotearoa New Zealand peatlands provides a proxy for temperature and growing-season energy availability rather than for precipitation or water balance.

This temperature signal represents a notable contrast with the widely studied *Sphagnum*-dominated peatland systems, where $\delta^{13}C$ in cellulose is typically linked primarily to water table depth and surface wetness rather than temperature (Loader et al., 2016; Loisel et al., 2009). The mechanistic basis for this contrast is well-grounded: *Sphagnum* mosses lack stomata and regulate water loss primarily through capillary evaporation from the capitulum, so their carbon discrimination responds to surface wetness via photosynthetic rate and CO_2 supply (Loader et al., 2016). *Empodisma*, a vascular plant with stomatal control and high water-use efficiency, operates in a fundamentally different ecophysiological regime. Provided the peatland water table remains near the surface, as at most *Empodisma*-dominated sites, growing-season water stress does not occur, and carbon discrimination is governed primarily by temperature and light (PAR_0, GDD_0) rather than by stomatal closure under water deficit. This is consistent with Amesbury et al. (2015b) and with evidence that plant functional type and hydrology strongly influence cellulose isotope signals, particularly in *Sphagnum*-dominated systems (Túri et al., 2021).

The absence of moisture control at the site scale (all moisture correlations non-significant) is matched by a modest but significant sample-level WTD effect. This scale dependency, detectable at the within-site sample level but absent between sites, indicates that microhabitat hydrology influences carbon discrimination locally, but that this hydrological noise is swamped by the temperature signal when comparing across the full latitudinal transect. For downcore applications, this implies that large (>1 ‰) multi-decadal shifts in $\delta^{13}C$ are more plausibly attributed to temperature change than to WTD variation, whereas smaller centennial-scale oscillations may reflect a mixture of both, particularly if companion WTD proxies (e.g. testate amoebae, peat humification) indicate concurrent hydrological shifts, consistent with the established value of multiproxy approaches in peat palaeoclimate reconstruction.

The species effect on $\delta^{13}C$ (*E. robustum* mean -26.56 ‰ vs *E. minus* mean -25.72 ‰ root, $p = 0.016$) is collinear with latitude and cannot be separated from the climatic gradient in the current dataset. Possible physiological explanations include differences in mesophyll conductance, carboxylation capacity, or the effective growing season temperature window between the two species. The 0.84 ‰ mean species offset in root cellulose is comparable in magnitude to the WTD effect over the full sample-level range and to the variability within a single site and must be accounted for when comparing downcore $\delta^{13}C$ records from sites dominated by different species or experiencing past species transitions.

The systematic enrichment of shoot cellulose relative to root cellulose (1.25 ‰, $p < 0.001$) is consistent across all sites and both species. Possible explanations include differences in the timing and integration of cellulose formation between shoots and roots, or *Empodisma*-specific differences in post-photosynthetic carbohydrate allocation and metabolism. We note that the direction of this offset runs counter to the more commonly reported pattern in C_3 plants, in which heterotrophic tissues,

https://doi.org/10.5194/egusphere-2026-4962
Preprint. Discussion started: 25 August 2026

including roots, are ^{13}C-enriched relative to photosynthetic tissues through post-photosynthetic fractionation, which would predict enrichment of roots rather than shoots (Cernusak et al., 2009). Although direct analogues for shoot-root $\delta^{13}C$ offsets in peatland vascular plants are limited, peatland cellulose-isotope studies have shown that species identity and plant part can introduce systematic offsets that must be considered when comparing records across tissues and taxa (Jones et al., 2019; Sakurai et al., 2021).

4.4. Implications for interpreting downcore *Empodisma* records

The modern calibration developed here reframes how downcore *Empodisma* root cellulose $\delta^{18}O$ should be interpreted. The finding from Amesbury et al. (2015a) that root-associated water tracks precipitation isotopic composition was an important first step, but it did not resolve the relationship between that water and cellulose. The present study demonstrates that root cellulose $\delta^{18}O$ cannot be interpreted as a direct recorder of precipitation $\delta^{18}O$. Rather, it reflects a mixed internal plant-water signal in which both root and shoot tissues contribute in proportions that vary with species identity, season, and possibly climate-driven changes in plant physiology. The effective source water is more enriched than precipitation as a result of internal transport, evaporative enrichment, and biosynthetic fractionation, and the magnitude of enrichment varies between *E. robustum* and *E. minus* in a predictable and species-consistent way.

For palaeoclimate application, this has two key practical implications. First, the identity of the peat-forming material must be established for any downcore sequence used for $\delta^{18}O$ reconstruction. Given the disjunct distributions of the two species either side of the Kauri line, a switch between *E. robustum* and *E. minus* at a single site is unlikely; the more plausible complication is a downcore transition from *Empodisma* to another peat-forming taxon altogether. A core dominated by *E. robustum* is expected to have a higher f_A (greater root-water contribution) and thus a $\delta^{18}O$ signal more directly linked to the isotopic composition of root zone water, which in turn tracks precipitation more faithfully. A core dominated by *E. minus* is expected to have a lower f_A and a signal more weighted towards shoot water, which may integrate a different seasonal window and show greater evaporative enrichment. Second, any change in the dominant *Empodisma* species within a downcore sequence could produce a step-change in the $\delta^{18}O$ baseline that could be difficult to distinguish from a precipitation-driven signal without macrofossil evidence. This need to account for species identity is analogous to the species-specific caution highlighted in Sphagnum isotope studies, where both $\delta^{13}C$ and $\delta^{18}O$ relationships vary between taxa and reconstructions are therefore recommended to be species-specific (Granath et al., 2018)

The dual-proxy advantage of simultaneously measuring $\delta^{13}C$ and $\delta^{18}O$ on the same core material is important. If $\delta^{13}C$ provides a relatively direct temperature signal and $\delta^{18}O$ provides a more complex moisture-source signal mediated through internal plant-water dynamics, then divergence between the two records in a downcore sequence may identify periods when temperature and atmospheric circulation changed independently; the kind of signal that could help distinguish between different SAM-forcing interpretations. Periods of cooling with enriched $\delta^{18}O$ (suggesting changed moisture source despite cooling) would be especially informative. The downcore records from TNG and OTT (Sect. 3.3) suggest that this

https://doi.org/10.5194/egusphere-2026-4962
Preprint. Discussion started: 25 August 2026

complementarity may already be detectable over the 20th century instrumental period, though attribution is complicated by the concurrent IPO transition.

4.5. Twentieth-century isotope trends and their relationship to the SAM

The 20th-century downcore records from TNG and OTT provide partial but meaningful support for hypothesis H4. Interpreting them requires care in distinguishing two different axes of variation in $\delta^{13}C$. The calibration developed in Sects. 3.1 and 3.2 is spatial, established across a contemporary latitudinal gradient along which atmospheric CO_2 is common to all sites, so the $\delta^{13}C$-temperature relationship it describes is a between-site relationship at essentially fixed CO_2. The downcore records are temporal, and across the industrial period they carry an additional forcing that the spatial calibration cannot contain: the rise in atmospheric CO_2 and the accompanying decline in its $\delta^{13}C$. A downcore $\delta^{13}C$ trend therefore cannot be read directly against the spatial temperature calibration without first accounting for both. The modern calibration and IsoGSM composites establish that positive SAM phases tend to bring settled, high-pressure conditions to Aotearoa New Zealand with sporadically delivered, isotopically depleted southerly-derived precipitation, while negative SAM phases tend to bring enhanced westerlies, more frequent precipitation, and a greater relative influence of lower-latitude moisture sources. More broadly, negative SAM states have been linked to more equatorward moisture sourcing in Antarctic precipitation, by about 2.4° of latitude on average, likely through amplified planetary wave activity (Gao et al., 2024). This differs from the simple poleward-shift interpretation applied to higher-latitude Southern Hemisphere settings and instead reflects Aotearoa New Zealand 's position near the northern edge of the westerly wind belt.

Both $\delta^{18}O$ records show a coherent enrichment trend from approximately 1960-1975 onwards, with larger amplitude at OTT than TNG. However, the direction of this enrichment, towards more positive $\delta^{18}O$, is not consistent with the positive SAM trend, which should produce depleted precipitation at both sites under the moisture-source framework. This inconsistency partly reflects the difficulty of attributing 20th century Aotearoa New Zealand climate change to a single mode: the 1976-1977 IPO phase shift was associated with marked changes in Aotearoa New Zealand circulation and precipitation patterns (Salinger et al., 2001), while more recent warm extremes reflect the combined influence of IPO, ENSO, SAM and anthropogenic warming (Henley, 2017; Salinger et al., 2024). More fundamentally, the coupled enrichment in both $\delta^{13}C$ and $\delta^{18}O$ over the industrial period may reflect a common physiological response to rising atmospheric CO_2. This is a separate effect from the change in the isotopic composition of atmospheric CO_2 over the same period, for which the records have already been corrected: the Suess correction removes the atmospheric composition signal, whereas the physiological response described here follows from concentration. At a given assimilation rate, reduced stomatal conductance increases intrinsic water-use efficiency and reduces discrimination against ^{13}C, while associated changes in leaf-water enrichment can also act to increase cellulose $\delta^{18}O$. Because this provides a common directional forcing on both proxies at both sites, and coincides with the interval of instrumental SAM variability, the enrichment trends cannot be read as a direct expression of the SAM moisture-source signal. A further possibility, not resolvable with these data, is that warming has lengthened the

https://doi.org/10.5194/egusphere-2026-4962
Preprint. Discussion started: 25 August 2026

period over which assimilation can proceed at low rates, so that the integrated $\delta^{13}C$ signal reflects a change in the seasonal window of carbon fixation as well as in instantaneous discrimination (Campbell et al., 2014).

The mixing model results provide the most direct explanation for the between-site contrast, and one that follows from the modern calibration itself. OTT is dominated by *E. minus* with a substantially lower f_A (0.414), meaning its $\delta^{18}O$ signal is substantially weighted towards internal shoot water, which is more susceptible to evaporative enrichment. If the post-1977 climate shift at OTT involved warmer and/or drier growing seasons, this could have increased evaporative enrichment of shoot water and thereby enriched cellulose $\delta^{18}O$ through the plant-physiological pathway rather than through changes in precipitation $\delta^{18}O$ alone. Distinguishing between these two mechanisms will require companion proxies, particularly hydrological indicators such as testate amoebae WTD reconstructions from the same cores, and where possible independent temperature-sensitive records.

At TNG, the measured $\delta^{13}C$ record spans -28.24 to -27.04 ‰ in the most recent decade (2009-2016); once corrected for the Suess effect, the record enriches by +1.28 ‰ across the 1970 boundary, opposite in direction to the warming-driven depletion predicted by the calibration (warmer growing seasons → more discrimination → more negative $\delta^{13}C$). Comparable speleothem $\delta^{18}O$ records from Waitomo, approximately 130 km southwest of TNG, show coherent Holocene climate signals linked to atmospheric circulation and Tasman Sea influences, with the Waitomo record interpreted as sensitive to changes in the subtropical front and Tasman Front (Lorrey et al., 2020). The emerging picture from multiple proxy systems in the northern Aotearoa New Zealand region is therefore broadly coherent, although the *Empodisma* peat cellulose records presented here remain a pilot downcore application focused on the instrumental period.

The absence of a directional trend in the measured OTT $\delta^{13}C$ record is largely an artefact of the atmospheric Suess effect: once corrected, OTT shows an enrichment of +0.85 ‰ between the pre- and post-1970 periods, comparable in direction to TNG (+1.28 ‰) though smaller in magnitude. Mean land temperature across Aotearoa New Zealand, as represented by the homogenised seven-station series, increased by 0.92°C per century over 1909-2015 (Ministry of the Environment, 2018; Mullan et al., 2010). Because warming increases discrimination and therefore depletes cellulose $\delta^{13}C$, the enrichment recorded at both sites over this interval runs counter to the temperature control identified in the spatial calibration and cannot be explained by it. Spatially heterogeneous climate responses to SAM and IPO across Aotearoa New Zealand (Kidston et al., 2009; Salinger et al., 2001) may nonetheless contribute to differences in the expression of these signals between the two sites.

H4, that downcore cellulose $\delta^{13}C$ and $\delta^{18}O$ from contrasting sites behave as predicted by the surface calibration, is therefore only partially supported, and not in the way anticipated. The *Empodisma* systems record coherent, well-dated multi-decadal variability in both proxies at both sites, and the between-site contrast in $\delta^{18}O$ amplitude follows the species-dependent source-water partitioning established by the modern calibration. However, once the atmospheric Suess effect is removed, both proxies enrich monotonically at both sites over the industrial period, which is opposite in direction to the SAM expectation for $\delta^{18}O$ and to the temperature expectation for $\delta^{13}C$, and the direction that would be expected from rising atmospheric CO_2. We therefore interpret the pilot records as demonstrating proxy fidelity and mechanistic continuity with

https://doi.org/10.5194/egusphere-2026-4962
Preprint. Discussion started: 25 August 2026

the modern calibration, rather than as a SAM reconstruction. Isolating a circulation signal will require records extending before the industrial period, where the CO_2 trend is absent – precisely the Holocene sequences these sites preserve.

4.6. Towards Holocene SAM reconstruction from Aotearoa New Zealand peatlands

The modern calibration presented here provides the mechanistic foundation for extending the *Empodisma* isotope records through the full Holocene, with the goal of contributing an independent SAM reconstruction from a region and proxy archive currently absent from the Southern Hemisphere palaeoclimate network. Existing Common Era and Holocene reconstructions of Southern Hemisphere westerly wind and SAM-related circulation variability are dominated by records from southern South America, the sub-Antarctic islands, and Antarctica, all of which reflect the SAM signal from the high-latitude side of the pressure dipole (Fletcher and Moreno, 2012; Perren et al., 2020; Xia et al., 2018). Aotearoa New Zealand peatland records would provide a complementary mid-latitude perspective from the northern edge of the westerly wind belt, where the SAM signal is expressed differently and where the IsoGSM simulations predict isotopically distinct responses in the two principal growth regimes relevant to *E. robustum* and *E. minus*.

Several challenges must be addressed to realise this potential. A central issue is species constancy – macrofossil and pollen evidence from the full core sequences at TNG and OTT must document any past changes in the dominant peat-forming vegetation, and where possible in the identity of the dominant restiad taxa, as demonstrated by existing macrofossil, cuticle, and pollen work on northern Aotearoa New Zealand bog vegetation (Haenfling et al., 2016; Newnham et al., 2019). The mixing model results presented here show that species identity has a first-order effect on cellulose $\delta^{18}O$ through source-water partitioning, and any undetected species transition in the downcore record would produce an artefactual $\delta^{18}O$ shift. Second, the temperature dependence of the biochemical fractionation factor ε_b must be better constrained for *Empodisma* specifically, as discussed in Sect. 4.2; this affects quantitative $\delta^{18}O$ reconstruction at cold South Island sites in particular. Third, IPO and ENSO must be separated from SAM in multi-decadal reconstructions, which will require either very long records spanning much of the Holocene, or multi-site synthesis comparing records from regions with contrasting SAM, IPO, and ENSO sensitivities. The 13-site calibration network established here provides a strong spatial framework for addressing those differential sensitivities, suggesting that a multi-core approach, combining TNG and OTT at minimum, and ideally additional sites from the transect, would yield the most robust attribution .

Finally, the pairing of $\delta^{13}C$ and $\delta^{18}O$ on the same downcore material, as demonstrated here, offers a pathway to separating temperature and circulation signals that single-proxy records cannot achieve. The atmospheric part of that problem, the '^{13}C Suess effect', is corrected here. If its physiological counterpart, the iWUE (intrinsic water-use efficiency) trend, can also be constrained (Lavergne et al., 2019; McCarroll et al., 2009), then the $\delta^{13}C$-temperature calibration established in Sect. 3.2 can be applied downcore, and $\delta^{13}C$ provides an independent constraint on past temperature change (Lavergne et al., 2019; McCarroll et al., 2009)that can be used to account for the temperature component of the $\delta^{18}O$ record, isolating the moisture-source/circulation component. Paired cellulose $\delta^{13}C$ and $\delta^{18}O$ measurements have been explored in other vascular-plant peatland systems (Yu et al., 2011, 2013; Shi et al., 2019), although quantitative separation of temperature and moisture-

https://doi.org/10.5194/egusphere-2026-4962
Preprint. Discussion started: 25 August 2026

source effects remains an area of ongoing development (Kock et al., 2019a). In our view, this provides a coherent, internally consistent framework for quantitative palaeoclimate reconstruction from *Empodisma* cellulose.

5. Conclusions

Using an expanded spatial dataset of 13 sites spanning more than 11° of latitude, a monthly monitoring dataset at two contrasting sites, and cryogenic vacuum distillation of internal plant waters, this study established a modern calibration framework for stable carbon ($\delta^{13}C$) and oxygen ($\delta^{18}O$) isotope proxies in *Empodisma*-dominated peatlands in Aotearoa New Zealand. The key conclusions are as follows:

Hypothesis 1 (confirmed): The negative relationships between *Empodisma* cellulose $\delta^{13}C$ and temperature and energy variables identified in the earlier six-site pilot study (Amesbury et al., 2015b) are replicated across the expanded dataset with substantially greater statistical power. Root cellulose $\delta^{13}C$ correlates significantly with both mean annual temperature ($r = -0.613$, $p = 0.034$) and mean summer temperature ($r = -0.628$, $p = 0.029$) across 12 sites, and the relationship is stronger for shoot cellulose. No significant associations with any moisture variable are found at the site scale, confirming the decoupling of $\delta^{13}C$ from direct hydrological controls across this latitudinal transect. For $\delta^{18}O$, the earlier finding that peatland waters track precipitation isotopic composition and plot close to the GMWL is confirmed and extended across all 13 sites, with the updated peatland MWL slope (8.80) reflecting the revised exclusion of internal shoot water from the peatland water definition.

Hypothesis 2 (confirmed). Root-associated water and internal root water $\delta^{18}O$ are significantly and positively related across the combined spatial and temporal datasets ($r = 0.719$, $p < 0.001$, $n = 63$), confirming that external peatland source-water signals are transmitted into internal plant water pools. However, internal root water is systematically depleted relative to root-associated water (mean $\delta^{18}O$ offset 2.98 ‰), and the magnitude of this fractionation differs significantly between species (*E. robustum* 3.89 ‰ vs *E. minus* 2.46 ‰, $p = 0.033$). These results demonstrate that root-associated water and internal root water are closely coupled but not interchangeable, and that the degree of isotopic modification between external and internal plant-water pools is species-dependent.

Hypothesis 3 (confirmed). The mean of internal root and internal shoot water is the best-performing candidate source water in the mechanistic model comparison, producing a near-zero mean offset in the spatial dataset (+0.59 ‰) and the smallest mean offset in the temporal dataset (-2.26 ‰), and substantially outperforming each alternative candidate source water tested, including either internal water pool individually. This result indicates that root cellulose $\delta^{18}O$ in *Empodisma* reflects a mixed internal plant-water source in which both root and shoot tissues contribute to the substrate available for cellulose synthesis. Quantification of source-water partitioning via isotope mixing reveals a global spatial optimum of $f_A = 0.627$, but with systematic species differences (*E. robustum* $f_A = 0.770$; *E. minus* $f_A = 0.414$) and a pronounced seasonal shift at the North Island monitoring site (NovMar $f_A = 0.700$; AprOct $f_A = 0.086$). Root cellulose $\delta^{18}O$ in *Empodisma* should not

https://doi.org/10.5194/egusphere-2026-4962
Preprint. Discussion started: 25 August 2026

therefore be treated as a direct recorder of precipitation $\delta^{18}O$; it is an integrated proxy for peatland source-water state mediated through species-specific and seasonally variable internal plant-water dynamics.

Hypothesis 4 (partially supported). Downcore root cellulose $\delta^{18}O$ and $\delta^{13}C$ records from Tangonge (North Island, *E. robustum*) and Otautau (South Island, *E. minus*) both register coherent, well-dated multi-decadal signals over the period c. 1900-2017 CE. The between-site contrast in $\delta^{18}O$ amplitude follows the species-dependent source-water partitioning established by the modern calibration, with the larger signal at OTT consistent with the substantially lower root-water fraction of *E. minus* and its corresponding greater shoot-water weighting. The direction of change, however, is not what the SAM framework predicts: once corrected for the atmospheric Suess effect, both proxies enrich at both sites over the industrial period, opposite to the depletion that would be expected under a positive SAM trend and in the direction that would be expected from rising atmospheric CO_2. Attribution of the 20th century isotope trends to SAM specifically therefore cannot be achieved from a single 120-year record, given the concurrent IPO phase shift, greenhouse warming and CO_2 rise. The coherent signals nonetheless demonstrate that the archived cellulose preserves reproducible isotopic information and that the calibration framework established here provides a robust basis for interpretation of pre-industrial sequences, where the CO_2 trend is absent.

Overall, the results establish *Empodisma* cellulose $\delta^{13}C$ and $\delta^{18}O$ as complementary palaeoclimate proxies with distinct but interpretable proxy frameworks: $\delta^{13}C$ primarily records growing-season temperature and energy availability, while $\delta^{18}O$ records peatland source-water state and its large-scale atmospheric circulation controls, filtered through species-specific internal plant-water dynamics. This dual-proxy framework provides the mechanistic basis for applying *Empodisma* cellulose isotopes to Holocene-length downcore records as proxies for past Southern Annular Mode variability. Aotearoa New Zealand's restiad peatlands are amongst the country's most widespread and well-preserved Holocene archives, yet their potential as stable isotope palaeoclimate archives remains largely unrealised. The calibration presented here addresses that gap directly, providing the species-specific, mechanistically grounded framework needed to unlock these archives and add a distinctive vascular plant peatland perspective to the growing multi-proxy network documenting past SAM variability across Aotearoa New Zealand and the broader Southern Hemisphere mid-latitudes.

Code availability

No new code was developed for this study. Age-depth models were produced using the published R package rplum (version 0.1.4; Aquino-López et al., 2018). Figures were produced in R (version 4.5.2; R Core Team, 2025) using ggplot2 (version 4.0.2; Wickham, 2016) and patchwork (version 1.3.2; Pederson, 2025); LOESS smoothers were fitted using the loess function of the stats package. All other analyses used standard statistical procedures described in Sect. 2.7 and can be reproduced from the data and equations given in the text.

https://doi.org/10.5194/egusphere-2026-4962
Preprint. Discussion started: 25 August 2026

Data availability

All cellulose and water stable isotope measurements, site metadata and chronological data generated in this study will be deposited in Zenodo and made publicly available upon publication. Precipitation isoscape values are from Baisden et al. (2016). Climate data are from the NIWA Virtual Climate Station Network. Atmospheric $\delta^{13}C\text{-}CO_2$ values are from Graven et al. (2017). The SAM index of Marshall (2003) is available at https://legacy.bas.ac.uk/met/gjma/sam.html.

Author contributions

DJC, TPR, MJA, JR, HG, and RMN conceived the study. DJC, TPR, and MJA acquired funding and administered the project. TPR, MJA, RMN, ABHR, JLR, and DJC undertook fieldwork and sample collection. TPR, MJA, JR, EDK, WTVB, MB, and MAA-L performed formal analysis. All authors contributed to the study methodology. TPR prepared the original draft, with contributions from MJA. All authors reviewed and edited the manuscript.

Competing interests

The authors declare that they have no conflicts of interest.

Statement on inclusion in global research

This research was led from the United Kingdom and carried out in Aotearoa New Zealand, with Aotearoa New Zealand-based researchers involved as collaborators from the project's inception and as co-authors. Fieldwork was undertaken on the lands of Te Rarawa, Ngāi Takoto, and Ngāti Rangi with the agreement and support of tangata whenua, and our project was discussed with iwi representatives at a Te Hiku o Te Ika research hui in Kaitaia. Local knowledge shared by iwi members informed site selection and fieldwork. Sampling was carried out under permits issued by the Department of Conservation. All contributors are named in the acknowledgements.

Acknowledgements

We are extremely grateful to the iwi of Te Hiku o Te Ika, and in particular to Te Rarawa, especially Waikarere Gregory, Ngāi Takoto, and Ngāti Rangi, for generously providing access to their land and for their advice and support throughout this work; we are also grateful for the hospitality we received at Te Rarawa marae at Pukepoto. We thank Wendy Hendwood and Te Hiku o Te Ika Iwi Development Trust for inviting us to discuss our research at the Research Hui on environmental issues in Kaitaia. We thank Kaio Hooper (Ngāi Takoto) for his help with fieldwork and local knowledge. We thank the staff at Te Ahu Museum, Kaitaia, for sharing photographs and records relating to Tangonge. We are grateful to the Department of

https://doi.org/10.5194/egusphere-2026-4962
Preprint. Discussion started: 25 August 2026

Conservation for granting research permits (Authorisation 52381-FLO) and to DOC staff for on-site support, and to Landcorp for access to Sweetwater Station and other farmland. We also thank Kevin Matthews for valuable local advice, and Paul Stevens for facilitating access to Tahakopa. During the preparation of this manuscript, the authors used Claude (Opus 5, Anthropic) to independently verify numerical calculations and check internal consistency of reported values. All outputs were checked against the underlying data by the authors, who take full responsibility for the content of this manuscript.

Financial support

This research has been supported by the Leverhulme Trust (grant no. RPG-2015-394).

References

Abram, N. J., Mulvaney, R., Vimeux, F., Phipps, S. J., Turner, J., and England, M. H.: Evolution of the Southern Annular Mode during the past millennium, Nat. Clim. Chang., 4, 564–569, https://doi.org/10.1038/nclimate2235, 2014.

Amesbury, M. J., Charman, D. J., Newnham, R. M., Loader, N. J., Goodrich, J., Royles, J., Campbell, D. I., Keller, E. D., Baisden, W. T., Roland, T. P., and Gallego-Sala, A. V.: Can oxygen stable isotopes be used to track precipitation moisture source in vascular plant-dominated peatlands?, Earth Planet. Sci. Lett., 430, 149–159, https://doi.org/10.1016/j.epsl.2015.08.015, 2015a.

Amesbury, M. J., Charman, D. J., Newnham, R. M., Loader, N. J., Goodrich, J. P., Royles, J., Campbell, D. I., Roland, T. P., and Gallego-Sala, A.: Carbon stable isotopes as a palaeoclimate proxy in vascular plant dominated peatlands, Geochim. Cosmochim. Acta, 164, 161–174, https://doi.org/10.1016/j.gca.2015.05.011, 2015b.

Anderson, H. J., Moy, C. M., Vandergoes, M. J., Nichols, J. E., Riesselman, C. R., and Hale, R. V.: Southern Hemisphere westerly wind influence on southern New Zealand hydrology during the Lateglacial and Holocene, J. Quat. Sci., 33, 689–701, https://doi.org/10.1002/jqs.3045, 2018.

Appleby, P. G. and Oldfield, F.: The calculation of lead-210 dates assuming a constant rate of supply of unsupported 210Pb to the sediment, CATENA, 5, 1–8, https://doi.org/10.1016/s0341-8162(78)80002-2, 1978.

Aquino-López, M. A., Blaauw, M., Christen, J. A., and Sanderson, N. K.: Bayesian Analysis of 210Pb Dating, J. Agric., Biol. Environ. Stat., 23, 317–333, https://doi.org/10.1007/s13253-018-0328-7, 2018.

Arblaster, J. M. and Meehl, G. A.: Contributions of External Forcings to Southern Annular Mode Trends, J. Clim., 19, 2896–2905, https://doi.org/10.1175/jcli3774.1, 2006.

Baisden, W. T., Keller, E. D., Hale, R. V., Frew, R. D., and Wassenaar, L. I.: Precipitation isoscapes for New Zealand: enhanced temporal detail using precipitation-weighted daily climatology†, Isot. Environ. Heal. Stud., 52, 343–352, https://doi.org/10.1080/10256016.2016.1153472, 2016.

https://doi.org/10.5194/egusphere-2026-4962
Preprint. Discussion started: 25 August 2026

Banerjee, A., Fyfe, J. C., Polvani, L. M., Waugh, D., and Chang, K.-L.: A pause in Southern Hemisphere circulation trends due to the Montreal Protocol, Nature, 579, 544–548, https://doi.org/10.1038/s41586-020-2120-4, 2020.

Barbour, M. M.: Stable oxygen isotope composition of plant tissue: a review, Funct. Plant Biol., 34, 83–94, https://doi.org/10.1071/fp06228, 2007.

Berkelhammer, M., Stott, L., Yoshimura, K., Johnson, K., and Sinha, A.: Synoptic and mesoscale controls on the isotopic composition of precipitation in the western United States, Clim. Dyn., 38, 433–454, https://doi.org/10.1007/s00382-011-1262-3, 2012.

Bilali, H. E., Patterson, R. T., and Prokoph, A.: A Holocene paleoclimate reconstruction for eastern Canada based on δ18O cellulose of Sphagnum mosses from Mer Bleue Bog, Holocene, 23, 1260–1271, https://doi.org/10.1177/0959683613484617, 2013.

Buhay, W. M., Edwards, T. W. D., and Aravena, R.: Evaluating kinetic fractionation factors used for reconstructions from oxgen and hydrogen isotope ratios in plant water and cellulose, Geochim. Cosmochim. Acta, 60, 2209–2218, https://doi.org/10.1016/0016-7037(96)00073-7, 1996.

Campbell, D. I., Smith, J., Goodrich, J. P., Wall, A. M., and Schipper, L. A.: Year-round growing conditions explains large CO2 sink strength in a New Zealand raised peat bog, Agric. For. Meteorol., 192, 59–68, https://doi.org/10.1016/j.agrformet.2014.03.003, 2014.

Cernusak, L. A., Tcherkez, G., Keitel, C., Cornwell, W. K., Santiago, L. S., Knohl, A., Barbour, M. M., Williams, D. G., Reich, P. B., Ellsworth, D. S., Dawson, T. E., Griffiths, H. G., Farquhar, G. D., and Wright, I. J.: Why are non-photosynthetic tissues generally 13C enriched compared with leaves in C3 plants? Review and synthesis of current hypotheses, Funct. Plant Biol., 36, 199–213, https://doi.org/10.1071/fp08216, 2009.

Charman, D. J.: Modelling hydrological relationships of testate amoebae (Protozoa: Rhizopoda) on New Zealand peatlands, J. R. Soc. N. Zealand, 27, 465–483, https://doi.org/10.1080/03014223.1997.9517549, 1997.

Clarkson, B. R., Schipper, L. A., and Silvester, W. B.: Nutritional niche separation in coexisting bog species demonstrated by 15N-enriched simulated rainfall, Austral Ecol., 34, 377–385, https://doi.org/10.1111/j.1442-9993.2009.01939.x, 2009.

Clem, K. R. and Fogt, R. L.: Varying roles of ENSO and SAM on the Antarctic Peninsula climate in austral spring, J. Geophys. Res.: Atmos., 118, 11,481-11,492, https://doi.org/10.1002/jgrd.50860, 2013.

Coplen, T. B.: Guidelines and recommended terms for expression of stable-isotope-ratio and gas-ratio measurement results, Rapid Commun. Mass Spectrom., 25, 2538–2560, https://doi.org/10.1002/rcm.5129, 2011.

Daley, T. J., Barber, K. E., Street-Perrott, F. A., Loader, N. J., Marshall, J. D., Crowley, S. F., and Fisher, E. H.: Holocene climate variability revealed by oxygen isotope analysis of Sphagnum cellulose from Walton Moss, northern England, Quat. Sci. Rev., 29, 1590–1601, https://doi.org/10.1016/j.quascirev.2009.09.017, 2010.

Dätwyler, C., Neukom, R., Abram, N. J., Gallant, A. J. E., Grosjean, M., Jacques-Coper, M., Karoly, D. J., and Villalba, R.: Teleconnection stationarity, variability and trends of the Southern Annular Mode (SAM) during the last millennium, Clim. Dyn., 51, 2321–2339, https://doi.org/10.1007/s00382-017-4015-0, 2018.

https://doi.org/10.5194/egusphere-2026-4962
Preprint. Discussion started: 25 August 2026

Dätwyler, C., Grosjean, M., Steiger, N. J., and Neukom, R.: Teleconnections and relationship between the El Niño–Southern Oscillation (ENSO) and the Southern Annular Mode (SAM) in reconstructions and models over the past millennium, Clim. Past, 16, 743–756, https://doi.org/10.5194/cp-16-743-2020, 2020.

Dee, S., Bailey, A., Conroy, J. L., Atwood, A., Stevenson, S., Nusbaumer, J., and Noone, D.: Water isotopes, climate variability, and the hydrological cycle: recent advances and new frontiers, Environ. Res.: Clim., 2, 022002, https://doi.org/10.1088/2752-5295/accbe1, 2023.

Ehleringer, J. R., Roden, J., and Dawson, T. E.: Methods in Ecosystem Science, 181–198, https://doi.org/10.1007/978-1-4612-1224-9_13, 2000.

Elliot, M. B.: Late Quaternary pollen records of vegetation and climate change from Kaitaia Bog, far northern New Zealand, Rev. Palaeobot. Palynol., 99, 189–202, https://doi.org/10.1016/s0034-6667(97)00048-1, 1998.

Ministry of the Environment: Climate Change Projections for New Zealand: Atmosphere Projections Based on Simulations from the IPCC Fifth Assessment, 2nd Edition, Ministry for the Environment, Wellington, 2018.

Estop-Aragonés, C., Cooper, M. D. A., Fisher, J. P., Thierry, A., Garnett, M. H., Charman, D. J., Murton, J. B., Phoenix, G. K., Treharne, R., Sanderson, N. K., Burn, C. R., Kokelj, S. V., Wolfe, S. A., Lewkowicz, A. G., Williams, M., and Hartley, I. P.: Limited release of previously-frozen C and increased new peat formation after thaw in permafrost peatlands, Soil Biol. Biochem., 118, 115–129, https://doi.org/10.1016/j.soilbio.2017.12.010, 2018.

Farquhar, G. D., Ehleringer, J. R., and Hubick, K. T.: Carbon Isotope Discrimination and Photosynthesis, Annu. Rev. Plant Physiol. Plant Mol. Biol., 40, 503–537, https://doi.org/10.1146/annurev.pp.40.060189.002443, 1989.

Fewster, R. E., Swindles, G. T., Carrivick, J. L., Gałka, M., Roland, T. P., McKeown, M., Sutherland, J. L., Tweed, F., Mullan, D., Graham, C., Gallego-Sala, A., and Morris, P. J.: Climate Warming and Deglaciation Drive New Peat Formation in the Southern Alps, Aotearoa/New Zealand, Geophys. Res. Lett., 52, https://doi.org/10.1029/2024gl113786, 2025.

Fletcher, M.-S. and Moreno, P. I.: Zonally symmetric changes in the strength and position of the Southern Westerlies drove atmospheric CO2 variations over the past 14 k.y., Geology, 39, 419–422, https://doi.org/10.1130/g31807.1, 2011.

Fletcher, M.-S. and Moreno, P. I.: Have the Southern Westerlies changed in a zonally symmetric manner over the last 14,000 years? A hemisphere-wide take on a controversial problem, Quat. Int., 253, 32–46, https://doi.org/10.1016/j.quaint.2011.04.042, 2012.

Fletcher, M.-S., Benson, A., Bowman, D. M. J. S., Gadd, P. S., Heijnis, H., Mariani, M., Saunders, K. M., Wolfe, B. B., and Zawadzki, A.: Centennial-scale trends in the Southern Annular Mode revealed by hemisphere-wide fire and hydroclimatic trends over the past 2400 years, Geology, 46, 363–366, https://doi.org/10.1130/g39661.1, 2018.

Fogt, R. L. and Marshall, G. J.: The Southern Annular Mode: Variability, trends, and climate impacts across the Southern Hemisphere, Wiley Interdiscip. Rev.: Clim. Chang., 11, https://doi.org/10.1002/wcc.652, 2020.

Frugone-Álvarez, M., Latorre, C., Giralt, S., Polanco-Martínez, J., Bernárdez, P., Oliva-Urcia, B., Maldonado, A., Carrevedo, M. L., Moreno, A., Huertas, A. D., Prego, R., Barreiro-Lostres, F., and Valero-Garcés, B.: A 7000-year high-

https://doi.org/10.5194/egusphere-2026-4962
Preprint. Discussion started: 25 August 2026

resolution lake sediment record from coastal central Chile (Lago Vichuquén, 34°S): implications for past sea level and environmental variability, J. Quat. Sci., 32, 830–844, https://doi.org/10.1002/jqs.2936, 2017.

Gallant, A. J. E., Phipps, S. J., Karoly, D. J., Mullan, A. B., and Lorrey, A. M.: Nonstationary Australasian Teleconnections and Implications for Paleoclimate Reconstructions, J. Clim., 26, 130627112859004, https://doi.org/10.1175/jcli-d-12-00338.1, 2013.

Gao, Q., Sime, L. C., McLaren, A. J., Bracegirdle, T. J., Capron, E., Rhodes, R. H., Steen-Larsen, H. C., Shi, X., and Werner, M.: Evaporative controls on Antarctic precipitation: an ECHAM6 model study using innovative water tracer diagnostics, Cryosphere, 18, 683–703, https://doi.org/10.5194/tc-18-683-2024, 2024.

Gibson, P. B., Stone, D., Thatcher, M., Broadbent, A., Dean, S., Rosier, S. M., Stuart, S., and Sood, A.: High-Resolution CCAM Simulations Over New Zealand and the South Pacific for the Detection and Attribution of Weather Extremes, J. Geophys. Res.: Atmos., 128, https://doi.org/10.1029/2023jd038530, 2023.

Gillett, N. P., Kell, T. D., and Jones, P. D.: Regional climate impacts of the Southern Annular Mode, Geophys. Res. Lett., 33, https://doi.org/10.1029/2006gl027721, 2006.

Granath, G., Rydin, H., Baltzer, J. L., Bengtsson, F., Boncek, N., Bragazza, L., Bu, Z.-J., Caporn, S. J. M., Dorrepaal, E., Galanina, O., Gałka, M., Ganeva, A., Gillikin, D. P., Goia, I., Goncharova, N., Hájek, M., Haraguchi, A., Harris, L. I., Humphreys, E., Jiroušek, M., Kajukało, K., Karofeld, E., Koronatova, N. G., Kosykh, N. P., Lamentowicz, M., Lapshina, E., Limpens, J., Linkosalmi, M., Ma, J.-Z., Mauritz, M., Munir, T. M., Natali, S. M., Natcheva, R., Noskova, M., Payne, R. J., Pilkington, K., Robinson, S., Robroek, B. J. M., Rochefort, L., Singer, D., Stenøien, H. K., Tuittila, E.-S., Vellak, K., Verheyden, A., Waddington, J. M., and Rice, S. K.: Environmental and taxonomic controls of carbon and oxygen stable isotope composition in Sphagnum across broad climatic and geographic ranges, Biogeosciences, 15, 5189–5202, https://doi.org/10.5194/bg-15-5189-2018, 2018.

Graven, H., Allison, C. E., Etheridge, D. M., Hammer, S., Keeling, R. F., Levin, I., Meijer, H. A. J., Rubino, M., Tans, P. P., Trudinger, C. M., Vaughn, B. H., and White, J. W. C.: Compiled records of carbon isotopes in atmospheric CO2 for historical simulations in CMIP6, Geosci. Model Dev., 10, 4405–4417, https://doi.org/10.5194/gmd-10-4405-2017, 2017.

Gruber, N., Landschützer, P., and Lovenduski, N. S.: The Variable Southern Ocean Carbon Sink, Annu. Rev. Mar. Sci., 11, 159–186, https://doi.org/10.1146/annurev-marine-121916-063407, 2018.

Haenfling, C., Newnham, R., Rees, A., Jara, I., Homes, A., and Clarkson, B.: Holocene history of a raised bog, northern New Zealand, based on plant cuticles, Holocene, 27, 309–314, https://doi.org/10.1177/0959683616658524, 2016.

Henley, B. J.: Pacific decadal climate variability: Indices, patterns and tropical-extratropical interactions, Glob. Planet. Chang., 155, 42–55, https://doi.org/10.1016/j.gloplacha.2017.06.004, 2017.

Hessl, A., Allen, K. J., Vance, T., Abram, N. J., and Saunders, K. M.: Reconstructions of the southern annular mode (SAM) during the last millennium, Prog. Phys. Geogr., 41, 834–849, https://doi.org/10.1177/0309133317743165, 2017.

https://doi.org/10.5194/egusphere-2026-4962
Preprint. Discussion started: 25 August 2026

Hinojosa, J. L., Moy, C. M., Stirling, C. H., Wilson, G. S., and Eglinton, T. I.: A New Zealand perspective on centennial-scale Southern Hemisphere westerly wind shifts during the last two millennia, Quat. Sci. Rev., 172, 32–43, https://doi.org/10.1016/j.quascirev.2017.07.016, 2017.

Hodgson, D. A. and Sime, L. C.: Southern westerlies and CO2, Nat. Geosci., 3, 666–667, https://doi.org/10.1038/ngeo970, 2010.

Ivanciu, I., Matthes, K., Wahl, S., Harlaß, J., and Biastoch, A.: Effects of prescribed CMIP6 ozone on simulating the Southern Hemisphere atmospheric circulation response to ozone depletion, Atmos. Chem. Phys., 21, 5777–5806, https://doi.org/10.5194/acp-21-5777-2021, 2021.

Jara, I. A., Newnham, R. M., Vandergoes, M. J., Foster, C. R., Lowe, D. J., Wilmshurst, J. M., Moreno, P. I., Renwick, J. A., and Homes, A. M.: Pollen–climate reconstruction from northern South Island, New Zealand (41°S), reveals varying high- and low-latitude teleconnections over the last 16 000 years, J. Quat. Sci., 30, 817–829, https://doi.org/10.1002/jqs.2818, 2015.

Jara, I. A., Newnham, R. M., Alloway, B. V., Wilmshurst, J. M., and Rees, A. B.: Pollen-based temperature and precipitation records of the past 14,600 years in northern New Zealand (37°S) and their linkages with the Southern Hemisphere atmospheric circulation, Holocene, 27, 1756–1768, https://doi.org/10.1177/0959683617708444, 2017.

Jones, M. C., Anderson, L., Keller, K., Nash, B., Littell, V., Wooller, M., and Jolley, C. A.: An Assessment of Plant Species Differences on Cellulose Oxygen Isotopes From Two Kenai Peninsula, Alaska Peatlands: Implications for Hydroclimatic Reconstructions, Front. Earth Sci., 7, 25, https://doi.org/10.3389/feart.2019.00025, 2019.

Kaplan, J. O., Bigelow, N. H., Prentice, I. C., Harrison, S. P., Bartlein, P. J., Christensen, T. R., Cramer, W., Matveyeva, N. V., McGuire, A. D., Murray, D. F., Razzhivin, V. Y., Smith, B., Walker, D. A., Anderson, P. M., Andreev, A. A., Brubaker, L. B., Edwards, M. E., and Lozhkin, A. V.: Climate change and Arctic ecosystems: 2. Modeling, paleodata-model comparisons, and future projections, J. Geophys. Res.: Atmos., 108, https://doi.org/10.1029/2002jd002559, 2003.

Kidson, J. W.: An analysis of New Zealand synoptic types and their use in defining weather regimes, Int. J. Clim., 20, 299–316, https://doi.org/10.1002/(sici)1097-0088(20000315)20:3<299::aid-joc474>3.0.co;2-b, 2000.

Kidston, J., Renwick, J. A., and McGregor, J.: Hemispheric-Scale Seasonality of the Southern Annular Mode and Impacts on the Climate of New Zealand, J. Clim., 22, 4759–4770, https://doi.org/10.1175/2009jcli2640.1, 2009.

King, J., Anchukaitis, K. J., Allen, K., Vance, T., and Hessl, A.: Trends and variability in the Southern Annular Mode over the Common Era, Nat. Commun., 14, 2324, https://doi.org/10.1038/s41467-023-37643-1, 2023.

Kock, S. T., Schittek, K., Mächtle, B., Wissel, H., Maldonado, A., and Lücke, A.: Late Holocene environmental changes reconstructed from stable isotope and geochemical records from a cushion-plant peatland in the Chilean Central Andes (27°S), J. Quat. Sci., 34, 153–164, https://doi.org/10.1002/jqs.3088, 2019a.

Kock, S. T., Schittek, K., Wissel, H., Vos, H., Ohlendorf, C., Schäbitz, F., Lupo, L. C., Kulemeyer, J. J., and Lücke, A.: Stable Oxygen Isotope Records (δ18O) of a High-Andean Cushion Peatland in NW Argentina (24° S) Imply South

https://doi.org/10.5194/egusphere-2026-4962
Preprint. Discussion started: 25 August 2026

American Summer Monsoon Related Moisture Changes During the Late Holocene, Front. Earth Sci., 7, 45, https://doi.org/10.3389/feart.2019.00045, 2019b.

Koffman, B. G., Kreutz, K. J., Breton, D. J., Kane, E. J., Winski, D. A., Birkel, S. D., Kurbatov, A. V., and Handley, M. J.: Centennial-scale variability of the Southern Hemisphere westerly wind belt in the eastern Pacific over the past two millennia, Clim. Past, 10, 1125–1144, https://doi.org/10.5194/cp-10-1125-2014, 2014.

Landschützer, P., Gruber, N., Haumann, F. A., Rödenbeck, C., Bakker, D. C. E., Heuven, S. van, Hoppema, M., Metzl, N., Sweeney, C., Takahashi, T., Tilbrook, B., and Wanninkhof, R.: The reinvigoration of the Southern Ocean carbon sink, Science, 349, 1221–1224, https://doi.org/10.1126/science.aab2620, 2015.

Lara, A., Villalba, R., and Urrutia, R.: A 400-year tree-ring record of the Puelo River summer–fall streamflow in the Valdivian Rainforest eco-region, Chile, Clim. Chang., 86, 331–356, https://doi.org/10.1007/s10584-007-9287-7, 2008.

Lavergne, A., Graven, H., Kauwe, M. G. D., Keenan, T. F., Medlyn, B. E., and Prentice, I. C.: Observed and modelled historical trends in the water-use efficiency of plants and ecosystems, Glob. Chang. Biol., 25, 2242–2257, https://doi.org/10.1111/gcb.14634, 2019.

Li, N. and McGregor, G. R.: Linking interannual river flow river variability across New Zealand to the Southern Annular Mode, 1979–2011, Hydrol. Process., 31, 2261–2276, https://doi.org/10.1002/hyp.11184, 2017.

Lim, E., Hendon, H. H., Arblaster, J. M., Delage, F., Nguyen, H., Min, S., and Wheeler, M. C.: The impact of the Southern Annular Mode on future changes in Southern Hemisphere rainfall, Geophys. Res. Lett., 43, 7160–7167, https://doi.org/10.1002/2016gl069453, 2016.

Loader, N. J., Robertson, I., Barker, A. C., Switsur, V. R., and Waterhouse, J. S.: An improved technique for the batch processing of small wholewood samples to α-cellulose, Chem. Geol., 136, 313–317, https://doi.org/10.1016/s0009-2541(96)00133-7, 1997.

Loader, N. J., Street-Perrott, F. A., Mauquoy, D., Roland, T. P., Bellen, S. van, Daley, T. J., Davies, D., Hughes, P. D. M., Pancotto, V. O., Young, G. H. F., Amesbury, M. J., Charman, D. J., Mallon, G., and Yu, Z. C.: Measurements of hydrogen, oxygen and carbon isotope variability in Sphagnum moss along a micro-topographical gradient in a southern Patagonian peatland, J. Quat. Sci., 31, 426–435, https://doi.org/10.1002/jqs.2871, 2016.

Loisel, J., Garneau, M., and Hélie, J.: Modern Sphagnumδ13C signatures follow a surface moisture gradient in two boreal peat bogs, James Bay lowlands, Québec, J. Quat. Sci., 24, 209–214, https://doi.org/10.1002/jqs.1221, 2009.

Loisel, J., Garneau, M., and Hélie, J.-F.: Sphagnum δ13C values as indicators of palaeohydrological changes in a peat bog, Holocene, 20, 285–291, https://doi.org/10.1177/0959683609350389, 2010.

Lorrey, A. M., Williams, P. W., Woolley, J.-M., Fauchereau, N. C., Hartland, A., Bostock, H., Eaves, S., Lachniet, M. S., Renwick, J. A., and Varma, V.: Late Quaternary Climate Variability and Change from Aotearoa New Zealand Speleothems: Progress in Age Modelling, Oxygen Isotope Master Record Construction and Proxy-Model Comparisons, Quaternary, 3, 24, https://doi.org/10.3390/quat3030024, 2020.

https://doi.org/10.5194/egusphere-2026-4962
Preprint. Discussion started: 25 August 2026

Marshall, G. J.: Trends in the Southern Annular Mode from Observations and Reanalyses, J. Clim., 16, 4134–4143, https://doi.org/10.1175/1520-0442(2003)016<4134:titsam>2.0.co;2, 2003.

Mathison, K.: OIA request response: Use of "Aotearoa New Zealand" in Ministry publications [Official Information Act response, 12 August 2021], https://environment.govt.nz/assets/publications/OIAD-21-To-publish.pdf, 2021.

McCarroll, D., Gagen, M. H., Loader, N. J., Robertson, I., Anchukaitis, K. J., Los, S., Young, G. H. F., Jalkanen, R., Kirchhefer, A., and Waterhouse, J. S.: Correction of tree ring stable carbon isotope chronologies for changes in the carbon dioxide content of the atmosphere, Geochim. Cosmochim. Acta, 73, 1539–1547, https://doi.org/10.1016/j.gca.2008.11.041, 2009.

McKinley, G. A., Pilcher, D. J., Fay, A. R., Lindsay, K., Long, M. C., and Lovenduski, N. S.: Timescales for detection of trends in the ocean carbon sink, Nature, 530, 469–472, https://doi.org/10.1038/nature16958, 2016.

Moreno, P. I., Francois, J. P., Moy, C. M., and Villa-Martínez, R.: Covariability of the Southern Westerlies and atmospheric CO2 during the Holocene, Geology, 38, 727–730, https://doi.org/10.1130/g30962.1, 2010.

Moreno, P. I., Vilanova, I., Villa-Martínez, R., Garreaud, R. D., Rojas, M., and Pol-Holz, R. D.: Southern Annular Mode-like changes in southwestern Patagonia at centennial timescales over the last three millennia, Nat. Commun., 5, 4375, https://doi.org/10.1038/ncomms5375, 2014.

Moreno, P. I., Vilanova, I., Villa-Martínez, R., Dunbar, R. B., Mucciarone, D. A., Kaplan, M. R., Garreaud, R. D., Rojas, M., Moy, C. M., Pol-Holz, R. D., and Lambert, F.: Onset and Evolution of Southern Annular Mode-Like Changes at Centennial Timescale, Sci. Rep., 8, 3458, https://doi.org/10.1038/s41598-018-21836-6, 2018.

Mullan, A. B., Stuart, S. J., Hadfield, M. G., and Smith, M. J.: Report on the Review of NIWA's "Seven-Station" Temperature Series, National Institute of Water and Atmospheric Research, Wellington, 2010.

Newnham, R. M., Lange, P. J. de, and Lowe, D. J.: Holocene vegetation, climate and history of a raised bog complex, northern New Zealand based on palynology, plant macrofossils and tephrochronology, Holocene, 5, 267–282, https://doi.org/10.1177/095968369500500302, 1995.

Newnham, R. M., Hazell, Z. J., Charman, D. J., Lowe, D. J., Rees, A. B. H., Amesbury, M. J., Roland, T. P., Gehrels, M., Bos, V. van den, and Jara, I. A.: Peat humification records from Restionaceae bogs in northern New Zealand as potential indicators of Holocene precipitation, seasonality, and ENSO, Quat. Sci. Rev., 218, 378–394, https://doi.org/10.1016/j.quascirev.2019.06.036, 2019.

Perren, B. B., Hodgson, D. A., Roberts, S. J., Sime, L., Nieuwenhuyze, W. V., Verleyen, E., and Vyverman, W.: Southward migration of the Southern Hemisphere westerly winds corresponds with warming climate over centennial timescales, Commun. Earth Environ., 1, 58, https://doi.org/10.1038/s43247-020-00059-6, 2020.

Phillips, D. L. and Gregg, J. W.: Uncertainty in source partitioning using stable isotopes, Oecologia, 127, 171–179, https://doi.org/10.1007/s004420000578, 2001.

https://doi.org/10.5194/egusphere-2026-4962
Preprint. Discussion started: 25 August 2026

Prentice, I. C., Cramer, W., Harrison, S. P., Leemans, R., Monserud, R. A., and Solomon, A. M.: Special Paper: A Global Biome Model Based on Plant Physiology and Dominance, Soil Properties and Climate, J. Biogeogr., 19, 117, https://doi.org/10.2307/2845499, 1992.

Rahaman, W., Chatterjee, S., Ejaz, T., and Thamban, M.: Increased influence of ENSO on Antarctic temperature since the Industrial Era, Sci. Rep., 9, 6006, https://doi.org/10.1038/s41598-019-42499-x, 2019.

Renwick, J. and Thompson, D.: The Southern Annular Mode and New Zealand climate, Water & Atmosphere, 2, 24–25, 2006.

Roden, J. S., Lin, G., and Ehleringer, J. R.: A mechanistic model for interpretation of hydrogen and oxygen isotope ratios in tree-ring cellulose, Geochim. Cosmochim. Acta, 64, 21–35, https://doi.org/10.1016/s0016-7037(99)00195-7, 2000.

Roland, T. P., Daley, T. J., Caseldine, C. J., Charman, D. J., Turney, C. S. M., Amesbury, M. J., Thompson, G. J., and Woodley, E. J.: The 5.2 ka climate event: Evidence from stable isotope and multi-proxy palaeoecological peatland records in Ireland, Quat. Sci. Rev., 124, 209–223, https://doi.org/10.1016/j.quascirev.2015.07.026, 2015.

Sakurai, H., Yamamoto, M., Seki, O., Omori, T., and Sato, T.: Cellulose Oxygen Isotopes of Sphagnum and Vascular Plants in a Peat Core Reveal Climate Change in Northern Japan Over the Past 2,000 Years, Geochem., Geophys., Geosystems, 22, https://doi.org/10.1029/2020gc009597, 2021.

Salinger, M. J., Renwick, J. A., and Mullan, A. B.: Interdecadal Pacific Oscillation and South Pacific climate, Int. J. Clim., 21, 1705–1721, https://doi.org/10.1002/joc.691, 2001.

Salinger, M. J., Renwick, J., Behrens, E., Mullan, A. B., Diamond, H. J., Sirguey, P., Smith, R. O., Trought, M. C. T., V, L. A., Cullen, N. J., Fitzharris, B. B., Hepburn, C. D., Parker, A. K., and Sutton, P. J.: The unprecedented coupled ocean-atmosphere summer heatwave in the New Zealand region 2017/18: drivers, mechanisms and impacts, Environ. Res. Lett., 14, 044023, https://doi.org/10.1088/1748-9326/ab012a, 2019.

Salinger, M. J., Trenberth, K. E., Diamond, H. J., Behrens, E., Fitzharris, B. B., Herold, N., Smith, R. O., Sutton, P. J., and Trought, M. C. T.: Climate Extremes in the New Zealand Region: Mechanisms, Impacts and Attribution, Int. J. Clim., 44, 5809–5824, https://doi.org/10.1002/joc.8667, 2024.

Saunders, K. M., Roberts, S. J., Perren, B., Butz, C., Sime, L., Davies, S., Nieuwenhuyze, W. V., Grosjean, M., and Hodgson, D. A.: Holocene dynamics of the Southern Hemisphere westerly winds and possible links to CO2 outgassing, Nat. Geosci., 11, 650–655, https://doi.org/10.1038/s41561-018-0186-5, 2018.

Shi, F., Rao, Z., Cao, J., Huang, C., Wu, D., Yang, W., and Sun, W.: Meltwater is the dominant water source controlling α-cellulose δ18O in a vascular-plant-dominated alpine peatland in the Altai Mountains, Central Asia, J. Hydrol., 572, 192–205, https://doi.org/10.1016/j.jhydrol.2019.02.030, 2019.

Speranskaya, L., Campbell, D. I., Lafleur, P. M., and Humphreys, E. R.: Peatland evaporation across hemispheres: contrasting controls and sensitivity to climate warming driven by plant functional types, Biogeosciences, 21, 1173–1190, https://doi.org/10.5194/bg-21-1173-2024, 2024.

https://doi.org/10.5194/egusphere-2026-4962
Preprint. Discussion started: 25 August 2026

Stelling, J. M. and Yu, Z.: Regional Climate Change Recorded in Moss Oxygen and Carbon Isotopes from a Late Holocene Peat Archive in the Western Antarctic Peninsula, Geosciences, 9, 282, https://doi.org/10.3390/geosciences9070282, 2019.

Sternberg, L. and Ellsworth, P. F. V.: Divergent Biochemical Fractionation, Not Convergent Temperature, Explains Cellulose Oxygen Isotope Enrichment across Latitudes, PLoS ONE, 6, e28040, https://doi.org/10.1371/journal.pone.0028040, 2011.

Stewart, K. D., Hogg, A. McC., England, M. H., and Waugh, D. W.: Response of the Southern Ocean Overturning Circulation to Extreme Southern Annular Mode Conditions, Geophys. Res. Lett., 47, https://doi.org/10.1029/2020gl091103, 2020.

Strother, S. L., Salzmann, U., Roberts, S. J., Hodgson, D. A., Woodward, J., Nieuwenhuyze, W. V., Verleyen, E., Vyverman, W., and Moreton, S. G.: Changes in Holocene climate and the intensity of Southern Hemisphere Westerly Winds based on a high-resolution palynological record from sub-Antarctic South Georgia, Holocene, 25, 263–279, https://doi.org/10.1177/0959683614557576, 2015.

Tait, A., Henderson, R., Turner, R., and Zheng, X.: Thin plate smoothing spline interpolation of daily rainfall for New Zealand using a climatological rainfall surface, Int. J. Clim., 26, 2097–2115, https://doi.org/10.1002/joc.1350, 2006.

Tait, A., Sturman, J., and Clark, M.: An assessment of the accuracy of interpolated daily rainfall for New Zealand, Journal of Hydrology (New Zealand), 52, 25–44, 2012.

Thompson, D. W. J., Solomon, S., Kushner, P. J., England, M. H., Grise, K. M., and Karoly, D. J.: Signatures of the Antarctic ozone hole in Southern Hemisphere surface climate change, Nat. Geosci., 4, 741–749, https://doi.org/10.1038/ngeo1296, 2011.

Thompson, M. A., Campbell, D. I., and Spronken-Smith, R. A.: Evaporation from natural and modified raised peat bogs in New Zealand, Agric. For. Meteorol., 95, 85–98, https://doi.org/10.1016/s0168-1923(99)00027-1, 1999.

Túri, M., Hubay, K., Molnár, M., Braun, M., László, E., Futó, I., and Palcsu, L.: Holocene paleoclimate inferred from stable isotope (δ18O and δ13C) values in Sphagnum cellulose, Mohos peat bog, Romania, J. Paleolimnol., 66, 229–248, https://doi.org/10.1007/s10933-021-00202-z, 2021.

Turney, C. S. M., McGlone, M., Palmer, J., Fogwill, C., Hogg, A., Thomas, Z. A., Lipson, M., Wilmshurst, J. M., Fenwick, P., Jones, R. T., Hines, B., and Clark, G. F.: Intensification of Southern Hemisphere westerly winds 2000–1000 years ago: evidence from the subantarctic Campbell and Auckland Islands (52–50°S), J. Quat. Sci., 31, 12–19, https://doi.org/10.1002/jqs.2828, 2016.

Turney, C. S. M., Wilmshurst, J. M., Jones, R. T., Wood, J. R., Palmer, J. G., Hogg, A. G., Fenwick, P., Crowley, S. F., Privat, K., and Thomas, Z.: Reconstructing atmospheric circulation over southern New Zealand: Establishment of modern westerly airflow 5500 years ago and implications for Southern Hemisphere Holocene climate change, Quat. Sci. Rev., 159, 77–87, https://doi.org/10.1016/j.quascirev.2016.12.017, 2017.

Ummenhofer, C. C. and England, M. H.: Interannual Extremes in New Zealand Precipitation Linked to Modes of Southern Hemisphere Climate Variability, J. Clim., 20, 5418–5440, https://doi.org/10.1175/2007jcli1430.1, 2007.

https://doi.org/10.5194/egusphere-2026-4962
Preprint. Discussion started: 25 August 2026

Ummenhofer, C. C., Gupta, A. S., and England, M. H.: Causes of Late Twentieth-Century Trends in New Zealand Precipitation, J. Clim., 22, 3–19, https://doi.org/10.1175/2008jcli2323.1, 2009.

Vera, C. S. and Osman, M.: Activity of the Southern Annular Mode during 2015–2016 El Niño event and its impact on Southern Hemisphere climate anomalies, Int. J. Clim., 38, e1288–e1295, https://doi.org/10.1002/joc.5419, 2018.

Villalba, R., Lara, A., Masiokas, M. H., Urrutia, R., Luckman, B. H., Marshall, G. J., Mundo, I. A., Christie, D. A., Cook, E. R., Neukom, R., Allen, K., Fenwick, P., Boninsegna, J. A., Srur, A. M., Morales, M. S., Araneo, D., Palmer, J. G., Cuq, E., Aravena, J. C., Holz, A., and LeQuesne, C.: Unusual Southern Hemisphere tree growth patterns induced by changes in the Southern Annular Mode, Nat. Geosci., 5, 793–798, https://doi.org/10.1038/ngeo1613, 2012.

Wagstaff, S. J. and Clarkson, B. R.: Systematics and ecology of the Australasian genus Empodisma (Restionaceae) and description of a new species from peatlands in northern New Zealand, PhytoKeys, 13, 39–79, https://doi.org/10.3897/phytokeys.13.3259, 2012.

West, A. G., Patrickson, S. J., and Ehleringer, J. R.: Water extraction times for plant and soil materials used in stable isotope analysis, Rapid Commun. Mass Spectrom., 20, 1317–1321, https://doi.org/10.1002/rcm.2456, 2006.

Xia, Z., Yu, Z., and Loisel, J.: Centennial-scale dynamics of the Southern Hemisphere Westerly Winds across the Drake Passage over the past two millennia, Geology, 46, 855–858, https://doi.org/10.1130/g40187.1, 2018.

Yakir, D. and DeNiro, M. J.: Oxygen and Hydrogen Isotope Fractionation during Cellulose Metabolism in Lemna gibba L. 1, Plant Physiol., 93, 325–332, https://doi.org/10.1104/pp.93.1.325, 1990.

Yang, H., Johnson, K. R., Griffiths, M. L., and Yoshimura, K.: Interannual controls on oxygen isotope variability in Asian monsoon precipitation and implications for paleoclimate reconstructions, J. Geophys. Res.: Atmos., 121, 8410–8428, https://doi.org/10.1002/2015jd024683, 2016.

Yu, S.-Y.: Quantitative reconstruction of mid- to late-Holocene climate in NE China from peat cellulose stable oxygen and carbon isotope records and mechanistic models, Holocene, 23, 1507–1516, https://doi.org/10.1177/0959683613496292, 2013.

Yu, S.-Y., Kang, Z., and Zhou, W.: Quantitative palaeoclimate reconstruction as an inverse problem: A Bayesian inference of late-Holocene climate on the eastern Tibetan Plateau from a peat cellulose δ18O record, Holocene, 22, 405–412, https://doi.org/10.1177/0959683611425544, 2011.

Zanazzi, A. and Mora, G.: Paleoclimatic implications of the relationship between oxygen isotope ratios of moss cellulose and source water in wetlands of Lake Superior, Chem. Geol., 222, 281–291, https://doi.org/10.1016/j.chemgeo.2005.08.006, 2005.

Zeh, L., Igel, M. T., Schellekens, J., Limpens, J., Bragazza, L., and Kalbitz, K.: Vascular plants affect properties and decomposition of moss-dominated peat, particularly at elevated temperatures, Biogeosciences, 17, 4797–4813, https://doi.org/10.5194/bg-17-4797-2020, 2020.

https://doi.org/10.5194/egusphere-2026-4962
Preprint. Discussion started: 25 August 2026

Zhang, Z.-Y., Dao-Yi, G., Xue-Zhao, H., Yang-Na, L., and Sheng-Hui, F.: Statistical Reconstruction of the Antarctic Oscillation Index Based on Multiple Proxies, Atmos. Ocean. Sci. Lett., 3, 283–287, https://doi.org/10.1080/16742834.2010.11446883, 2015.